University of Alberta

The Mechanism of Sensitivity Reduction in Amorphous Selenium X-ray Detectors

by

Teodor Marius Stanescu 

A thesis submitted to the Faculty of Graduate Studies and Research in partial fulfillment of the requirements for the degree of Master of Science

in

Medical Physics

Department of Physics

Edmonton, Alberta

Fall 2004

Your file Votre référence
ISBN: 0-612-95857-4
Our file Notre référence
ISBN: 0-612-95857-4

Table of Contents

List of Tables

List of Figures

Chapter 1: Introduction

Amorphous selenium (a-Se) has been widely studied as a photodetector for applications in medical imaging[1-10] since the 1950s. Due to its favorable intrinsic properties, a-Se has been used for both optical and x-ray imaging. X-ray detectors based on a-Se are currently under study for diagnostic purposes, in the KeV energy range[11-14], and for the verification of radiotherapy treatments, in the MeV energy range. [15-18]

Digital images acquired on radiography systems with a-Se based detectors are susceptible to memory artifacts from prior x-rays exposures[19]. Experimentally, temporal artifacts such as sensitivity reduction[20] and lag[21,22] have been reported in externally-biased a-Se-based detectors in active matrix flat panels (AMFPs) that are being studied for medical imaging applications. These artifacts result in reduced contrast in the images subsequently produced by the detector. It is believed that the temporal artifacts are caused by the capture of charge carriers at local trapping sites.[20-22]

Even though a-Se was one of the best studied amorphous semiconductor material due to its xerographic importance[23,24] during 1970s, the relationship of the a-Se properties to its structure is still not fully understood.

1.1 Scope and organization of thesis

The main goal of this thesis is to investigate the x-ray sensitivity reduction effect of an a-Se parallel plate detector for different operating conditions.

A brief review of the main properties of a-Se as an x-ray photodetector and its applications in medical imaging are depicted in chapter 2. An overview of the x-ray sensitivity of a-Se considering recombination and trapping mechanisms is also presented.

Chapter 3 introduces the experimental methods and the materials used to quantify the reduction in sensitivity effect under various operating conditions. The a-Se detector and the setup used are described in detail. The x-ray sensitivity corresponding to the biased and non-biased cases is defined. The biased case refers to the condition when a potential is continuously applied across the photodetector's layer during the time of the experiment. The non-biased case is described by a sequence in which the detector is kept unbiased during fatiguing irradiation intervals, and biased only for the sensitivity probing with short irradiation pulses. The experimental sequences and the definitions of the sensitivity recovery corresponding to the bias and non-biased cases are also given in this chapter.

In chapter 4, a quantitative theory is developed to describe the mechanism of sensitivity reduction by considering that the photogenerated charge carriers can be captured in deep traps and become recombination centers for the subsequently generated opposite charge carriers. A system of partial differential equations along with initial and boundary conditions are introduced to describe the kinetics of the charge carriers, i.e. electrons and holes, in the a-Se photoconductor layer. An analytical solution for the total current density, defined as the sum of the conduction current and the displacement current densities is derived.

In chapter 5, the x-ray sensitivity response of a-Se parallel plate detectors is experimentally explored for different operating conditions, such as air-kerma rates, applied electric fields, and x-ray effective energies. The sensitivity was

measured for both the biased and non-biased cases. The sensitivity recovery was also investigated. Predicted and experimental dependences of the sensitivity upon the air-kerma, applied electric field, and x-ray effective energy are presented for the non-biased case. Sensitivity versus photodetector thickness profiles are theoretically derived for several x-ray effective photon energies. Also presented, are the theoretically-determined density of traps responsible for the reduction in sensitivity process, as well as, the numerical determined values of the trapping and recombination coefficients.

The conclusions of the thesis are summarized in Chapter 6.

1.2 References

1. R. M. Schaffert, R. C. McMaster, and W. E. Bixby, "Electroradiography," U.S. Patent 2666144 (1950).

2. W. Zhao, W. G. Ji, A. Debrie, and J. A. Rowlands, "Imaging performance of amorphous selenium based flat-panel detectors for digital mammography: Characterization of a small area prototype detector," Med. Phys. **30** (2), 254-263 (2003).

3. E. Samei and M. J. Flynn, "An experimental comparison of detector performance for direct and indirect digital radiography systems," Med. Phys. **30** (4), 608-622 (2003).

4 G. Pang, D. L. Lee, and J. A. Rowlands, "Investigation of a direct conversion flat panel imager for portal imaging," Med. Phys. **28** (10), 2121-2128 (2001).

5. W. Zhao, I. Blevis, S. Germann and J.A. Rowlands, "Digital radiology using active matrix readout of amorphous selenium: Construction and evaluation of a prototype real-time detector," Med. Phys. **24** 1834-1843 (1997).

6. Zhao and J.A. Rowlands, "X-ray imaging using amorphous selenium: Feasibility of a flat panel self-scanned detector for digital radiology," Med. Phys. **22** 1595-1604 (1995).

7. W. Zhao and J.A. Rowlands, "Digital radiology using active matrix readout of amorphous selenium: Theoretical analysis of detective quantum efficiency," Med. Phys. **24** 1819-1833 (1997).

8. M. Lachaine, "Portal Imaging with a Direct-Detection Active Matrix Flat Panel Imager", PhD Thesis (2001).

9. E. Fourkal, M. Lachaine, and B. G. Fallone, "Signal formation in amorphous-Se-based x-ray detectors", Phys. Rev. B **63** 195204.

10. A. Tsukamoto, S. Yamada, T. Tomisaki, M. Tanaka, T. Sakaguchi, H. Asahina, and M. Nishiki, "Development of a selenium-based flat-panel detector for real-time radiography and fluoroscopy," Proc. SPIE **3336**, 388-395 (1998).

11. B. Polischuk, H. Rougeot, K. Wong, A. Debrie, E. Poliquin, M. Hansroul, J. Martin, T. Truong, M. Choquette, L. Laperrière, and Z. Shukri, "Direct conversion detector for digital mammography," Proc. SPIE **3659**, 417-425 (1999).

12. L.E. Antonuk, Y. El-Mohri, J.H. Siewerdsen and J. Yorkston, "Empirical investigation of the signal performance of a high-resolution, indirect detection, active matrix flat-panel imager (AMFPI) for fluoroscopic and radiographic operation," Med. Phys. **24** 51-70 (1997).

13. J.H. Siewerdsen, L.E. Antonuk, Y. El-Mohri, J. Yorkston, W. Huang and J.M. Boudry, "Empirical and theoretical investigation of the noise performance of indirect detection, active matrix flat-panel imagers (AMFPIs) for diagnostic radiology," Med. Phys. **24** 71-89 (1997).

14. J.H. Siewerdsen, L.E. Antonuk, Y. El-Mohri, J. Yorkston and W. Huang, "Signal, noise power spectrum, and detective quantum efficiency of indirect-detection flat-panel imagers for diagnostic radiology," Med. Phys. **25** 614-628 (1998).

15. M. Lachaîne, E. Fourkal, and B. G. Fallone, "Investigation into the physical characteristics of active matrix flat panel imagers for radiotherapy," Med. Phys. **28** (8), 1689-1695 (2001).

16. M. Lachaîne, E. Fourkal, and B. G. Fallone, "Detective quantum efficiency of a direct-detection active matrix flat panel imager at megavoltage energies," Med. Phys. **28** (7), 1364-1372 (2001).

17. D. Mah, J.A. Rowlands and J.A. Rawlinson, "Sensitivity of amorphous selenium to x-rays from 40 kVp to 18 MV: Measurements and implications for portal imaging," Med. Phys. **25** 444-456 (1998).

18. L.E. Antonuk, Y. El-Mohri, W. Huang, K.-W. Jee, J. Siewerdsen, M. Maolinbay, V. Scarpine, H. Sandler and J. Yorkston, "Initial Performance Evaluation of an indirect detection, active matrix flat-panel imager (AMFPI) prototype for megavoltage imaging," Int. J. Rad. Onc. Biol. Phys. **42** 437-452 (1998).

19. H. G. Chotas et al, "Memory Artifacts Related to Selenium-based Digital Radiograph Systems", Radiology VOL. **203** No. 3 pp. 881-883 1997.

20. S. Steciw, T. Stanescu, S. Rathee, and B. G. Fallone, "Sensitivity Reduction in Biased Amorphous Selenium Photoconductors", J. Phys. D: Appl. Phys. **35**, 1 (2002).

21. W. Zhao, G. DeCrescenzo, and J. A. Rowlands, "Investigation of lag and ghosting in amorphous selenium flat-panel X-ray detectors", Proc. SPIE **4682**, 9 (2002).

22. C. Schroeder, T. Stanescu, S. Rathee and B. G. Fallone, "Lag measurement in an a-Se active matrix flat-panel imager", Med. Phys. **31** 5 1203 - 1209 (2004).

23. S. O. Kasap, "The Handbook of Imaging Materials", 2nd ed. A. Diamond, ed., Marcel Dekker, New York (1998), ch. 9 and references therein.

24. M. A. Abkowitz in Disordered Semiconductors, M. A. Kastner, G. A. Thomas, S. R. Ovshinsky, eds., Plenum Publishing, New York (1987), p. 205.

Chapter 2: Background

In this chapter a brief review of the main properties of a-Se as an x-ray photodetector along with its applications in medical imaging are considered. An overview of the x-ray sensitivity of a-Se with regards to recombination and trapping mechanisms is also presented.

2.1. Basic properties of a photodetector

A photodetector should present several unique properties in order to be a good choice for an x-ray detector with application in medical imaging, such as: high intrinsic x-ray sensitivity, negligible dark current, no trapping and recombination effects, negligible x-ray fatigue and x-ray damage.

The x-ray sensitivity can be quantified by considering the average energy required to create one electron-hole pair (EHP), W_0. Each x-ray photon, incident on a-Se layer, is able to generate many EHPs, in contrast to an optical photon which can produce only one EHP, due to its limited energy.

The value of W_0 can be described by a semi-empirical formula, given by Klein[1].

$$W_0 = 2.8E_g + E_{phonon} \tag{2.1}$$

where E_g, with a value of about $2.22\ eV$, is the a-Se band gap, and E_{phonon} is defined as the phonon contribution, and its value is expected to be small ($0.5\ eV$). Que and Rowlands[2] found that by relaxing the momentum conservation rule, as applied to amorphous semiconductors, W_0 would be described by the formula

$$W_0 = 2.2E_g + E_{phonon} \tag{2.2}$$

Considering the above scenarios, W_0 of a-Se can be estimated as being within $5-7\ eV$ range. The lower the value of W_0 the higher the number of free EHPs created per unit of incident radiation. Therefore a decrease of the band gap value will result in an increase of the collectable charge carriers (i.e. electrons and holes), which means a higher x-ray sensitivity. Due to its high atomic mass (78.96) and density ($4.2\ g/cm^3$), a-Se also shows a high x-ray sensitivity.

Ideally, there should be no dark current present in the photodetector. In a semiconductor, there are usually intermediate energy levels, given by intrinsic defects or dopping impurities, which act as the sources of thermally generated charge carriers (dark conductivity). In practice, we can minimize this effect by properly choosing the conditions required to manufacture the photodetector, such as deposition rate, substrate temperature and dopping concentrations. Another possible source of dark current is given by the contacts to the photoconductor. Charge carriers can be released in the photoconductor from the metal electrodes. As a solution, non-injecting or blocking electrical contacts are used in practice. This type of contacts are built by inserting, between the electrode and the photodetector, a very thin layer which allows the collection of charge carriers but blocks the transfer of charge from the electrode to the photodetector layer.[3]

A particular problem is found in electrostatic photoconductors, where a surface charge is present on the photodetector. The discharge of the surface potential in the case of no x-ray irradiation should be negligible.

Low dark current was noticed in materials with a large band gap, therefore this requirement opposes to the need of high intrinsic x-ray sensitivity. A-Se with

its band gap of about 2.22 eV meets well both requirements, showing very good x-ray sensitivity and also a low dark current (less than $1\,nA/cm^2$ at $E = 10\ V/\mu m$[4]).

The EHPs generated in the photodetector during irradiation are collected by applying a potential across the layer. The highest signal would be given by collecting all charge carriers released into the bulk. But due to the presence of intermediate energy levels in the semiconductor's band gap (i.e. a-Se), trapping and recombination processes usually take place. The magnitude of these effects depends mainly on the manufacturing process.

The preparation process is also important for a photodetector. Amorphous Se lacks the periodical atom structure present in crystals. Therefore it can be easily coated over large areas (desired characteristics in medical radiology), without altering its physical properties, through simple vacuum deposition techniques, and with low manufacturing costs.

2.2. Amorphous Se in medical imaging

Amorphous Selenium was originally used in xeroradiography, a medical imaging method introduced by Schaffert in 1950s[5]. An amorphous selenium layer is vacuum deposited onto an aluminum substrate in order to build an electroradiographic plate. In this design, a uniform positive charge is applied to the a-Se surface via corona-charging in order to sensitize the material, as shown in Fig. 2.1.

In effect, an electric field is established across the a-Se layer. When exposed to light or x-rays, the a-Se material acts as a photoconductor, generating free charge carriers, i.e. electron-hole pairs. This results in localized discharging of the plate proportional to the incident x-ray or optical light, and eventually forms a latent electrostatic image. Then toner particles are applied to the a-Se surface, and the latent image can be recorded on a special coated paper[5].

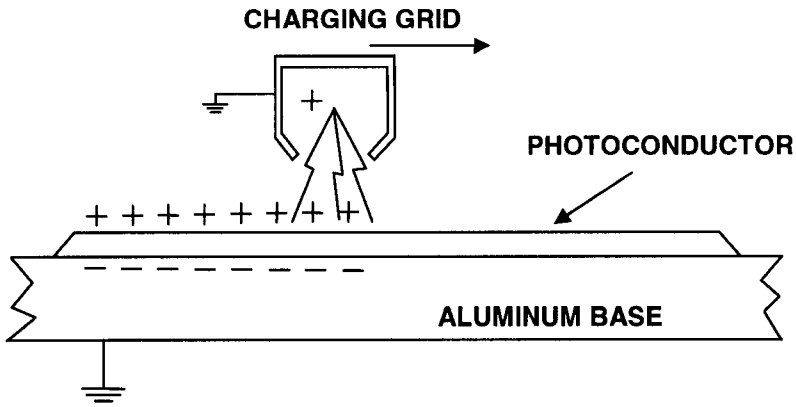

Figure 2.1. Sensitization of a xerographic plate by corona charging.

Interest in xeroradiography diminished due to the limitations in operating the equipment, in particular the toner deposition technique, rather than to the intrinsic properties of a-Se.

In recent years, technologies that allow real-time digital imaging, based on thin film transistors (TFTs), have been investigated[6-13]. Detectors, built as large active matrix arrays (AMAs) made out of individual TFTs (e.g. 30×30 cm^2) are able to produce digital x-ray images of high quality, allowing immediate visualization, processing and storage of the information of interest. This type of detector is usually called an active-matrix flat panel imager (AMFPI), and is based on two fundamentally different approaches of detecting x-rays: indirect[12-15] and direct[14-16] conversion.

In the first design, of an indirect AMFPI, the x-rays are converted into visible light by means of a phosphor screen (Gd_2O_2S) or a columnar structure of cesium iodine (CsI:Tl - better localization of the x-ray-induced scintillation light). Then the light generates charge carries into a photodetector pixel array, and the charge is subsequently read out with TFTs built on the same panels, to form a digital image (see Fig. 2.2a).

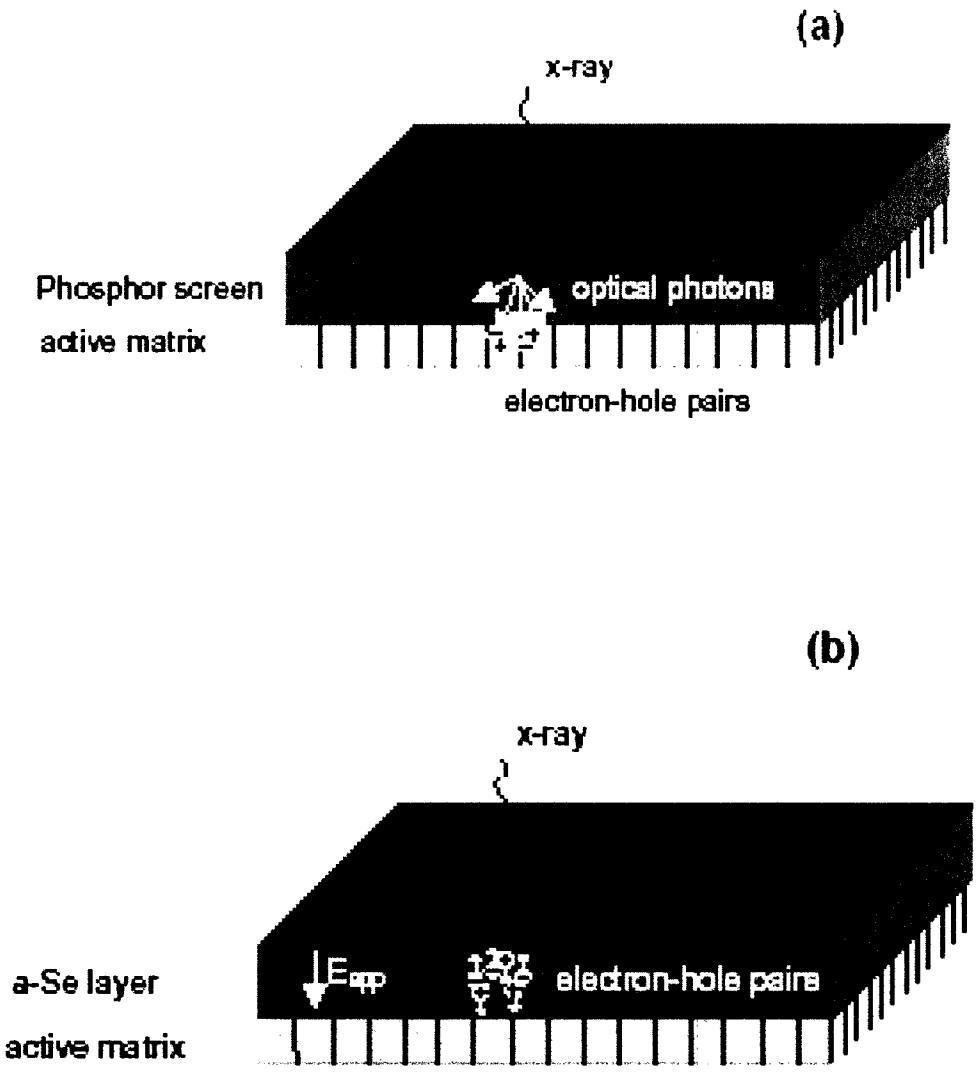

Figure 2.2. Schematic diagram showing an a) indirect AMFPI and b) direct AMFPI.

In direct AMFPIs, due to the interaction of x-rays with the photoconductor (i.e. a-Se), free charge carriers (EHPs) are generated within the layer, and subsequently collected through the use of an applied electric field by an array of pixel electrodes where the charge is stored by capacitors and subsequently read out to form the digital image (see Fig. 2.2b).

Comparing the two approaches, the indirect conversion method suffers from a loss in sensitivity and spatial resolution, a consequence of the scattering of light in the phosphor layer and the partial internal reflection of light in the columnar structure of cesium iodine.

In contrast, the direct conversion method avoids the limitations of two quantum conversion processes, the charge carriers being collected with negligible lateral spreading. The photodetector layer can be made thick enough to absorb the incident x-ray photons with negligible loss of resolution. In this case, the image resolution would be limited only by the granularity of the readout structure (i.e. pixel size).

In general, the advantages of a-Se include high resolution, suitable for medical imaging, and low noise. The advantages of the active matrix are real-time readout, flexible design parameters, and compactness of the readout structures.

Both AMFPI designs have been studied and successfully developed for various applications, in mammography, fluoroscopy and chest radiography.

2.3. X-ray sensitivity of a-Se

In the literature, the signal formation in a-Se is described through two different approaches. The first one, briefly presented in Section 2.3.1, refers to recombination mechanisms only, neglecting any trapping-related effects. In contrast, the second method covered in Section 2.3.2, describes the induced effects in a-Se due to charge carriers trapping and/or release processes.

2.3.1. Models based on recombination mechanisms

The recombination mechanisms developed to explain the signal formation in a-Se are based on the investigation of the average energy required to create a collectable EHP. This energy is defined by the following relationship

$$W_{\pm} = \frac{W_0}{\eta} \tag{2.3}$$

where W_0 is the average energy required to create an EHP (see Section 2.1), and η is the escape efficiency, which represents the fraction of EHPs which escape any perturbing effect, i.e. recombination or trapping, as they drift across the photoconductor. In this approach, it is assumed that charge carriers are lost only through recombination mechanisms, i.e. *general* and *initial recombination*[17], and any trapping effect is neglected.

General recombination, also called simple bulk or bimolecular recombination, takes place between any drifting electrons and holes generated inside the photodetector layer. Because its rate is proportional to both charge carriers concentrations, the collected charge does not increase linearly with the intensity of the irradiation (e.g. dose rate), having a rather square root dependence. However, experiments show that the measured charge collected is linear with the dose rate of the irradiation; therefore the general recombination process can be neglected.[43]

The initial recombination is based on the interaction between charge carriers generated along a single x-ray ionization track. Due to this fact, the initial recombination process does not depend on the intensity of irradiation, and needs to be considered.

For initial recombination, the interaction mechanism between freed electrons and holes is usually described by two competing models.

Hirsch and Jahankhani[18] suggested that the *columnar recombination* process described by Jaffe[19] is applicable to a-Se. This involves the recombination of the secondary charge carriers generated uniformly along the columnar track of a primary electron. The number of tracks is assumed to

increase proportionally with the dose rate, in agreement with the experimental observations. Kramers[20] extended this model in order to include a dependence on the electric field.

The second approach is *geminate recombination*, described by Que and Rowlands[2], and based on Onsager theory[21]. This mechanism involves only the mutual coulombic interaction between twin charge carriers, products of the same pair.

The debate on which recombination mechanism describes best the a-Se intrinsic properties evolved around two main issues: Onsager mechanism does not predict a dependence on mean photon energy, and columnar model does not assume any temperature dependence.

Blevis *et al*[22] showed from pulse height spectroscopy experiments that $W_{\pm}$ decreases with the increase of the mean x-ray photon energy (KeV), indicating that Onsager model is not applicable to the a-Se semiconductor. But recently, Mah *et al*[7] found experimentally that $W_{\pm}$ is independent of MeV energies. The latter authors considered that radiation deposits its energy in small spurs, and depending on its value the spurs can be treated as independent entities (high energies) or as interacting each other in a columnar track (low energies). On the other hand, even though Hirsch and Jahankhani[18] strongly supported through their experiments the columnar recombination mechanism, they were not able to explain the temperature dependence of the $W_{\pm}$.

Fourkal *et al*[23] developed a quantitative theory based on recombination mechanisms to describe the dependencies of $W_{\pm}$ on the applied field and the x-ray photon energy (both KeV and MeV ranges) which were experimentally found by Blevis *et al*[22] and Mah *et al*[24]. The approach follows the physical location of the charge carriers, i.e. electron-hole pairs, in a-Se layer in order to determine the fraction that escapes recombination and contributes to the detectable signal.

Although the recombination-based theoretical models describe reasonably well the experimental findings regarding $W_{\pm}$, they are not able to explain the memory artifacts present in a-Se detectors.

2.3.2. X-ray induced effects in a-Se

Experimental investigations with electroradiographic layers (ERLs) have shown that, although recombination has been proposed as a cause for the sensitivity reduction, x-ray induced trapping alone can lead to such an effect.[25-27] Xerographic techniques have indicated experimentally, that the deep-hole-trap population increases with exposure to x-ray.[26-28]

The density-of-states (DOS) diagram is a good guide for understanding the properties of a-Se.

Abkowitz[8] proposed the DOS diagram in Fig. 2.3, which is an extension of the Owen-Marshal's DOS model[9]. It was derived by combining results from a variety of experiments such as time-of-flight (TOF) drift mobility, xerographic cycled-up residual voltage decay and xerographic dark discharge measurements[8,10]. In this figure, the peak at 1.22 *eV* is responsible for the deep trapping of electrons and that at 0.87 *eV* for the deep trapping of holes.

Recently, Adriaenssens *et al* proposed a different DOS diagram, shown in Fig. 2.4, which is based on post-transient time transient photoconductivity measurements and analysis[11].

Chand *et al*[12] performed experiments on the thermally stimulated discharge (TSD) behavior of native (dark rested) and irradiated a-Se (99.999% pure) films, and found shallow and deep trapping levels for electrons at ~ 1.0 eV and ~ 1.6 eV , and for holes at ~ 1.0 eV and ~ 1.7 eV , respectively.

Chand *et al*[13] also studied the effect of chlorine dopping in a-Se. They found that by adding 30 *ppm* chlorine the trapping levels shifted to relatively shallower levels, i.e. from 1.6 eV and 1.7 eV to 1.4 eV and 1.5 eV for electrons and holes, respectively.

Kalade *et al*[29] reported the DOS diagram of Fig 2.5 for the 0.6 - 1.8 *eV* energy interval by using an optical excitation charge-carrier-filled states technique. The maximum density of the energy level distribution was found to be located at approximately 0.92 eV for electrons and 1.55 eV eV for holes. The authors also considered that localized hole states are expected at energies less than 0.6 eV .

These DOS characteristics exhibit different energy distributions of the electron and hole localized states, which lead to different interpretations for charge carriers transport and trapping.

It is well stated through experiment that the trapping states in the mobility gap, i.e. shallow and deep, are caused by the presence of structural defects that are thermodynamically stable at room temperature[30-33].

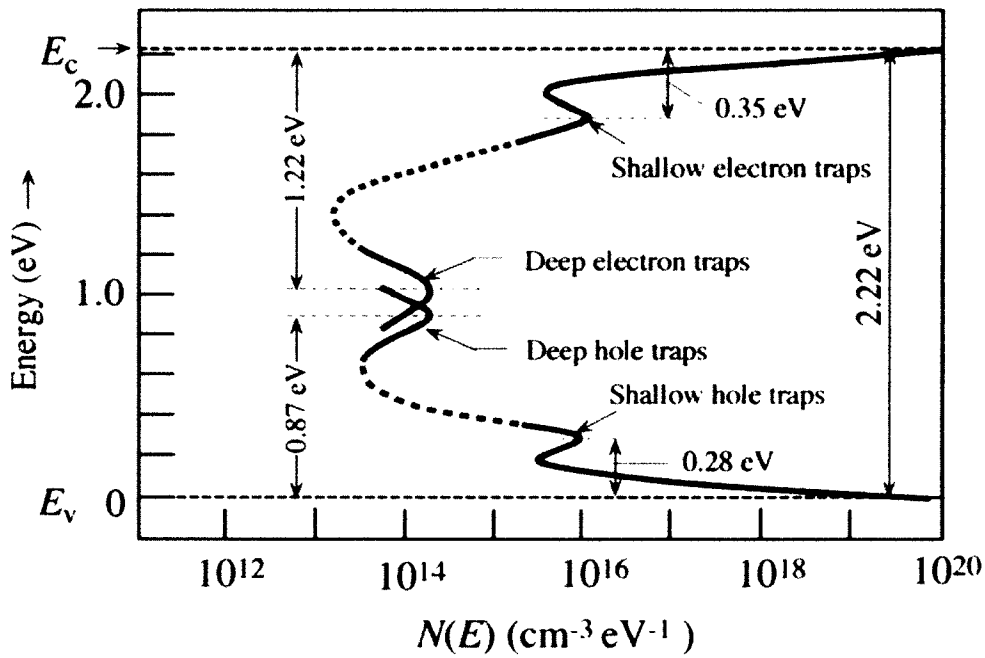

Figure 2.3. Density of states diagram after Abkowitz. N(E) is the density of localized states.

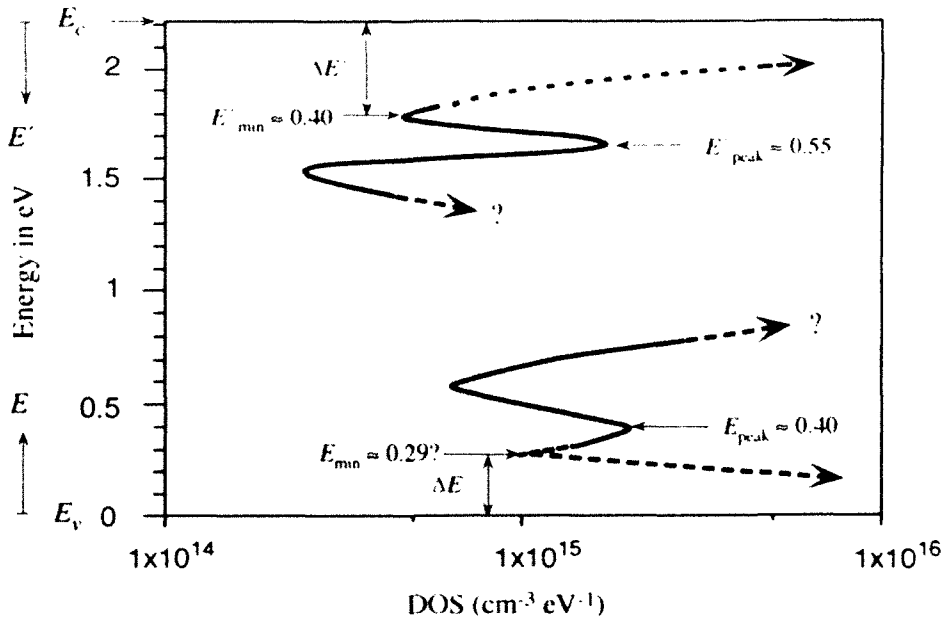

Figure 2.4. Density of states diagram after Adriaenssens *et al.*

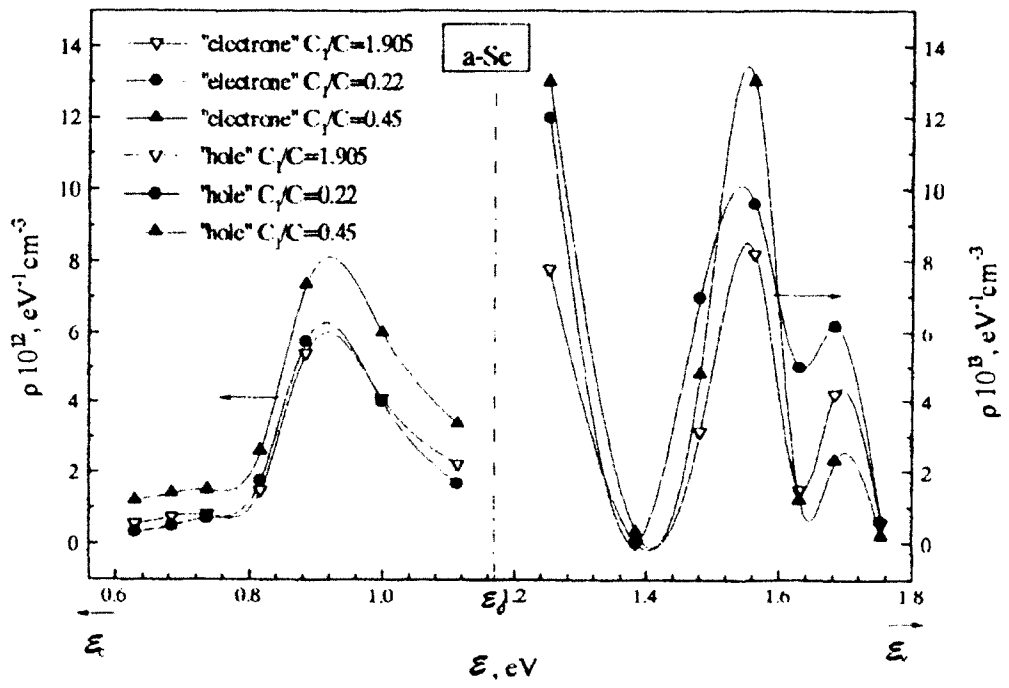

Figure 2.5. Density of states diagram after Kalade *et al.*

However, their exact mechanism is not well known. Research performed at Xerox[34,35] showed that the deep trapping states are equilibrium defects, and therefore their presence, can not be avoided by any means of purification or preparation processes. These trapping states control the carrier lifetimes and therefore the photodetector characteristics.

Although the sensitivity reduction has been studied for ERL's under various operating conditions including different detector thicknesses, applied electric fields, dose rates, and effective photon energies, to date, only scarce experimental[36] or theoretical studies have been performed for biased detectors.

2.4 References

1. 8. C.A. Klein, "Band gap dependence and related features of radiation ionization energies in semiconductors," J. Appl. Phys. **39** 2029 (1968).

2. 9. W. Que and J.A. Rowlands, "X-ray photogeneration in amorphous selenium: Geminate versus columnar recombination," Phys. Rev. B **51** 10500-10507 (1995).

3. A. Brauers, N. Conrads, G. Frings, U. Schiebel, M. J. Powell, and C. Glasse, "Charge Collection in a Se Photoconductor on a Thin Film Transistor Array During X-ray Imaging", Mat. Res. Soc.Symp. Proc. **467** 919-924 (1997).

4. 10. C. J. Haugen 1999, "X-ray Photoconductivity".

5. 11. R. M. Schaffert, R. C. McMaster, and W. E. Bixby, "Electroradiography," U.S. Patent 2666144 (1950).

6. 31. S. O. Kasap, "The Handbook of Imaging Materials", 2nd ed. A. Diamond, ed., Marcel Dekker, New York (1998), ch. 9 and references therein.

7. 32. M. A. Abkowitz in Disordered Semiconductors, M. A. Kastner, G. A. Thomas, S. R. Ovshinsky, eds., Plenum Publishing, New York (1987), p. 205.

8. 33. M. Abkowitz, "Density of states in a-Se from combined analysis of xerographic potentials and transient transport data," Philos. Mag. Lett. **58** (1), 53-57 (1988).

9. 34. Own A. E. and Marshall J. M., Proceedings on the Seventh International Conference on Amorphous and Liquid Semiconductors, Edinburgh (1977) p. 529.

10. 35. Kasap S. O., "The Handbook of Imaging Materials", ed. A. Diamond (Marcel Dekker, New York, 1991) ch. 8 and references therein.

11. 36. H.-Z. Song, G. J. Adriaenssens, E. V. Emelianova, and V. I. Arkhipov, "Distribution of gap states in amorphous delenium thin films", Phys. Rev. B **59** (1999) 10610.

12. 37. S. Chand, R. C. Bhatheja, G. D. Sharma, and S. Chandra, "Deep intrinsic and photostructural defects levels in amorphous selenium films", J. Appl. Phys. **70** (9) (1991) 5122-5124.

13. 38. S. Chand, R. C. Bhatheja, G. D. Sharma, and S. Chandra, "Effect of chlorine doping on photostructural defect states in amorphous selenium films", Appl. Phys. Lett. **59** (27) (1991) 3514-3515.

14. 16. W. Zhao, I. Blevis, S. Germann and J.A. Rowlands, "Digital radiology using active matrix readout of amorphous selenium: Construction and evaluation of a prototype realtime detector," Med. Phys. **24** 1834-1843 (1997).

15. 17. Zhao and J.A. Rowlands, "X-ray imaging using amorphous selenium: Feasibility of a flat panel self-scanned detector for digital radiology," Med. Phys. **22** 1595-1604 (1995).

16. 18. W. Zhao and J.A. Rowlands, "Digital radiology using active matrix readout of amorphous selenium: Theoretical analysis of detective quantum efficiency," Med. Phys. **24** 1819-1833 (1997).

17. 19. M. Lachaine, "Portal Imaging with a Direct-Detection Active Matrix Flat Panel Imager", PhD Thesis (2001).

18. 20. J. Hirsch and H. Jahankhani, "The carrier yield in a-Se under electron bombardment", J. Phys.: Condens. Matter **1** 8789 (1989).

19. 21. G. Jaffé, "Columnar ionization," Le Radium **10** 126-134 (1913).

20. 22. H.A. Kramers, "On a modification of Jaffé's theory of column ionization," Physica (Utrecht) **18** 665-675 (1952).

21. 23. D. M. Pai, R. C. Enck, "Onsager mechanism of photogeneration in amorphous selenium", Phys. Rev. B **11** (1975) 5163.

22. 24. I.M. Blevis, D.C. Hunt and J.A. Rowlands, "Measurement of x-ray photogeneration in amorphous selenium," J. Appl. Phys. **85** 7958-7963 (1999).

23. 25. E. Fourkal, M. Lachaine, and B. G. Fallone, "Signal formation in amorphous-Se-based x-ray detectors", Phys. Rev. B **63** 195204.

24. 7. D. Mah, J.A. Rowlands and J.A. Rawlinson, "Sensitivity of amorphous selenium to x-rays from 40 kVp to 18 MV: Measurements and implications for portal imaging," Med. Phys. **25** 444-456 (1998).

25. 46. J. Kalade, E. Montrimas and J. Rakauskas, "The Mechanism of Sensitivity Reduction in Selenium Layers Irradiated by X-Rays", Phys. Stat. Sol. A **25** 629 (1974).

26. 47. S. O. Kasap and V. Aiyah, "X-Ray induced hole trapping in electroradiographic plates", J. Appl. Phys. **69**, 7087 (1991).

27. 48. U. Schiebel, T. Buchkremer, G. Frings and P. Quadflieg, "Deep trapping and recombination in a-Se:As x-ray sensitive photoreceptors" J. Non-Cryst. Sol. **115**, 216 (1989).

28. 49. C. Haugen and S. O. Kasap, "X-ray irradiation induced bulk space charge in stabillized a-Se x-ray photoconductors", J Appl. Phys. **84** 5495, (1998).

29. 39. Kalade J. et al, "The deep localised state energetical distribution in a-Se and a-Si:H layers", Proc. SPIE **2780** (1996) 206-209.

30. 40. Wong C. K. et al, J. Non-Cryst. Solids **1171** 97-98 (1985).

31. 41. Veres J. and Juhasz C., J. Non-Cryst. Solids **407** 164-166 (1993).

32. 42. Abkowitz M. A., "Disordered Semiconductors", ed. Kastner M. A., Thomas G. A., and Ovshinsky S. R. (Plenum Publishing Co., New York, 1978) p. 205, and references therein.

33. 43. M. Abkowitz and J. M. Markovics, "Evidence of equilibrium native defect populations in amorphous chalcogenides from analyses of xerographic spectra", J. Non-Cryst. Solids **66** 315 (1984).

34. Adler D., "Amorphous Semiconductor Devices", Sci. Am. **36** 236 (1977).

35. Elliott S. R., "Physics of Amorphous Solids" (Longman, London, UK, 1992).

36. 28. S. Steciw, T. Stanescu, S. Rathee, and B. G. Fallone, "Sensitivity Reduction in Biased Amorphous Selenium Photoconductors", J. Phys. D: Appl. Phys. **35**, 1 (2002).

Chapter 3: Materials and Methods

This chapter presents the experimental methods used to quantify the reduction in sensitivity effect under various operating conditions. The amorphous selenium detector and the setup used for all our experiments are described in Section 3.1. The definitions of the x-ray sensitivity applied to the experimental sequences corresponding to the biased and non-biased cases are given in Section 3.2 and Section 3.3, respectively. The experimental sequences and the definitions of sensitivity recovery corresponding to the biased and non-biased cases are also presented in Section 3.2 and Section 3.3.

3.1. Experimental Apparatus

The apparatus used to irradiate and measure the collected current produced in the a-Se photoconductor[1] is presented in Fig. 3.1. The a-Se-based detector directly converts the x-rays into charge carriers, i.e. EHPs. Similar to the active-matrix flat panel imagers (AMFPIs), our a-Se detector, measuring $53 \times 26\ mm^2$, was constructed (Anrad Corporation, St-Laurent, Canada) on a $1\ mm$ thick glass substrate, where $239\ \mu m$ of a-Se (0.2% As) lay sandwiched between two parallel plate electrodes (Al and SnO_2), each $0.3\ \mu m$ thick.

A constant potential was applied to the electrodes using a Keithley 245 (Keithley Instruments Inc, Cleveland OH) high-voltage source. Considering that the average distance traveled by the electrons before being trapped (i.e.

Schubweg) is much smaller than for holes,[2,3] we wish the electrons to travel the shortest path in the photodetector layer. We applied the positive bias on the top electrode, facing the x-ray source. In this way, the electrons produced near the surface of the detector, especially during irradiation with low x-ray energy (e.g. 30KeV), are quickly collected and not captured into deep traps. However, for higher effective energies (e.g. 100 KeV), the generation of charge carriers inside the photodetector layer is uniform, therefore the collection efficiency is not significantly affected by the *Schubwegs* of electrons and holes.

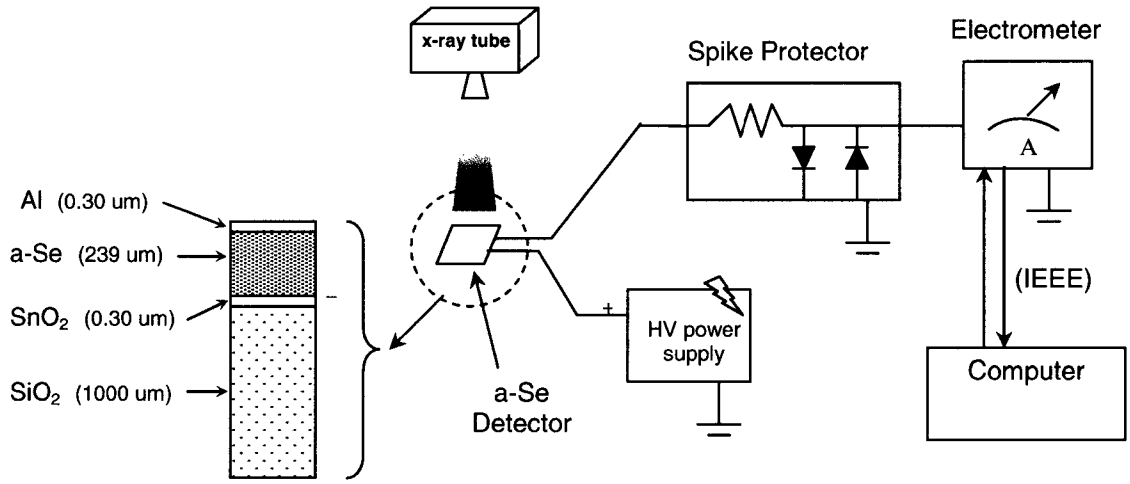

Figure 3.1. A block diagram showing HV power supply, a-Se detector, over-voltage protection circuit, electrometer and a host computer. The cross-section on left shows layers of glass substrate, a-Se and electrodes.

A-Se is also sensitive to exposure from optical photons. Therefore, the detector was placed in a light-tight cardboard box to avoid the generation of any unwanted charge carriers resulting from visible light.

The detector was irradiated by a superficial therapy 3 x-ray unit (Therapax, Pantak Inc, East Haven CT). We used both the *kVp* and the half-value layer (*HVL*) to describe the x-ray spectrum. The latter is defined as the

thickness of material required to reduce the x-ray fluence by one-half. The stability of the x-ray source was monitored and found to be approximately 1%.

The x-ray induced photocurrent, flowing through the detector, was measured by a Keithley 6514 electrometer (Keithley Instruments Inc, Cleveland OH) with a spike protector circuit to protect the electrometer from any over-current, and acquired on a computer via an IEEE interface card.

The electrometer was connected to a host PC (486D/33, Dell Computer Corp, Austin TX) via a GBIP IEEE interface card (National Instruments, Austin TX), where full control and data collection was accomplished using an in-house written C program.

All data was "time-stamped" by the electrometer, and later analyzed with the Matlab (MathWorks Inc, Natick MA) programming language.

3.2. X-ray sensitivity of an a-Se detector – biased case

3.2.1. Acquisition and Processing of Data

The reduction of sensitivity in a-Se was determined by measuring the response of a biased photoconductor to radiation. The x-ray sensitivity can be expressed in terms of the collected current as I/I_{max}, where I and I_{max} are the measured current value at any point in time during the irradiation process and the initial, i.e. maximum current measured, respectively. I_{max} is considered to be the photodetector response to x-ray irradiation in the absence of any trapping effect. The collected current was recorded during the irradiation for different air-kerma values, air-kerma rates, effective photon energies and applied electric fields during the irradiation.

The amplitude of the dark current varies with time during the irradiation. That is due to trapping and release effects of charge carriers from shallow traps. In order to subtract the dark current from the raw signal, the detector was

subjected to segmented irradiation intervals as depicted in Fig. 3.2. The dark current was determined and subsequently subtracted from each segment.

Due to release of charge carriers from shallow traps, the time interval between two subsequent irradiation segments was approximately 1 - 2 minutes to accurately record the dark current.

When multiple exposures were taken, we define $I_{\max}|_{i=1}$ as being the maximum current measured from the first exposure. The maximum value of the collected current in any subsequent irradiation segment is $I_{\max}|_i$, for $i > 1$.

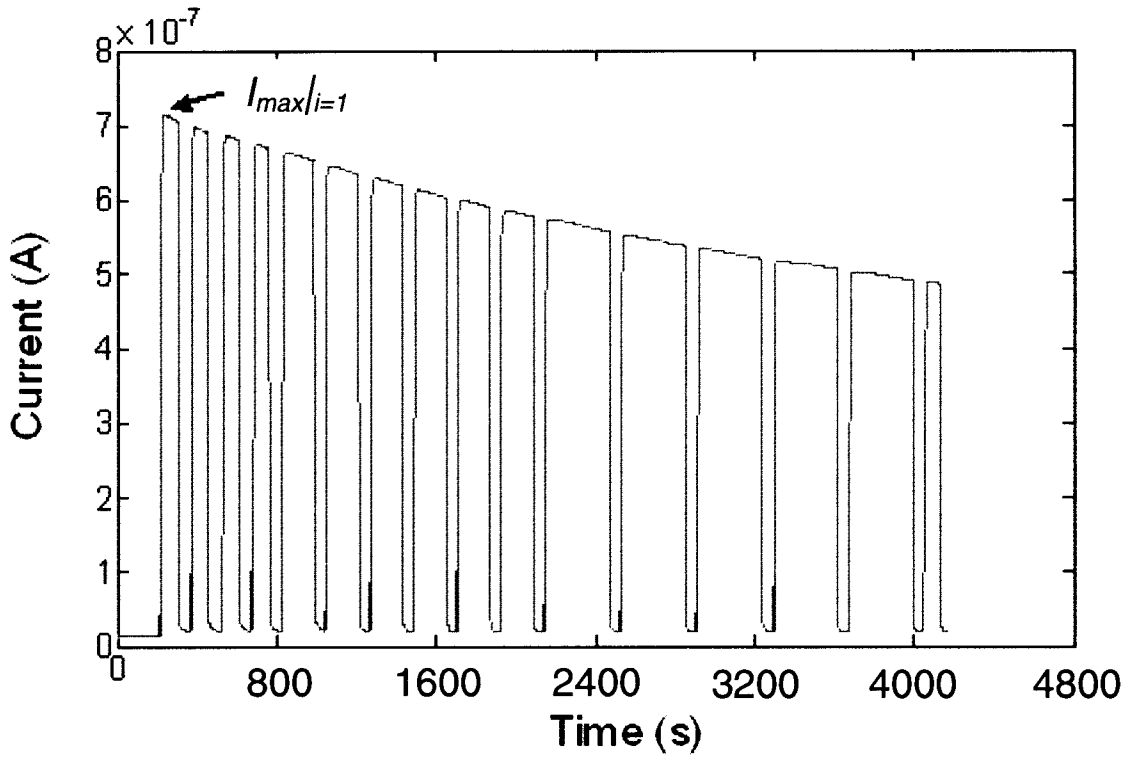

Figure 3.2. Typical raw signal from an a-Se detector for a segmented radiation delivery; $E = 4\ V/\mu m$, photon source = 75 *kVp* (*HVL* = 2.5 *mm* Al, where *HVL* is defined as thickness of material required to reduce the x-ray fluence by one-half), air-kerma rate $\dot{K} = 8.10\ cGy \cdot \min^{-1}$.

The dark current was measured just prior to each irradiation interval and subtracted from $I_{\max}|_i$, therefore giving the dark corrected current $I'_{\max}|_i$.

The detector's sensitivity corrected for dark current, after being irradiated during n segments, is given as follows

$$S_n = \frac{I'_{\max}|_i}{I'_{\max}|_{i=1}}, \text{ for } i \geq 1. \tag{3.1}$$

Sensitivity curves were generated from measured data using Eq. (3.1) as a function of delivered air-kerma for different air-kerma rates, x-ray effective photon energies, and applied electric field strengths. All measurements were made in a light-free environment with a constant bias, as shown in Fig. 3.1.

3.2.2. Acquisition and Processing of Data - Sensitivity Recovery

Once the a-Se detector has been irradiated, trapped charge carriers are released from trapping sites, and the sensitivity of the detector starts to increase for any subsequent irradiation, if enough time is given in between irradiations.

To quantify this recovery of sensitivity, the detector was initially subjected to a long irradiation interval ($i = 1$) by delivering a large air-kerma (i.e. 100 cGy), and followed by a short test measurement ($i = 2$) consisting of a small air-kerma (i.e. few cGy). The timing between the $i = 1$ and $i = 2$ irradiation intervals was about 2 seconds, representing the shortest time available on the irradiation unit.

The values of the collected current $I_{\max}|_{i=1}$ and $I_{\max}|_{i=2}$ corresponding to the first and the second segment were recorded, and then the detector was left biased over a certain time *t*. At the time *t*, the detector was once again irradiated with another test measurement ($i = 3$) and the collected current $I_{\max}|_{i=3}$ was recorded.

Figure 3.3 illustrates the segmented air-kerma delivery used to determine sensitivity recovery. Dark currents were subtracted from all $I_{\max}|_i$ values, and all measurements were made in light-tight cardboard box. The percent recovery was then determined as follows

$$\% \text{ recovery} = \frac{I'_{\max}|_{i=3} - I'_{\max}|_{i=2}}{I'_{\max}|_{i=1} - I'_{\max}|_{i=2}} \times 100\% . \tag{3.2}$$

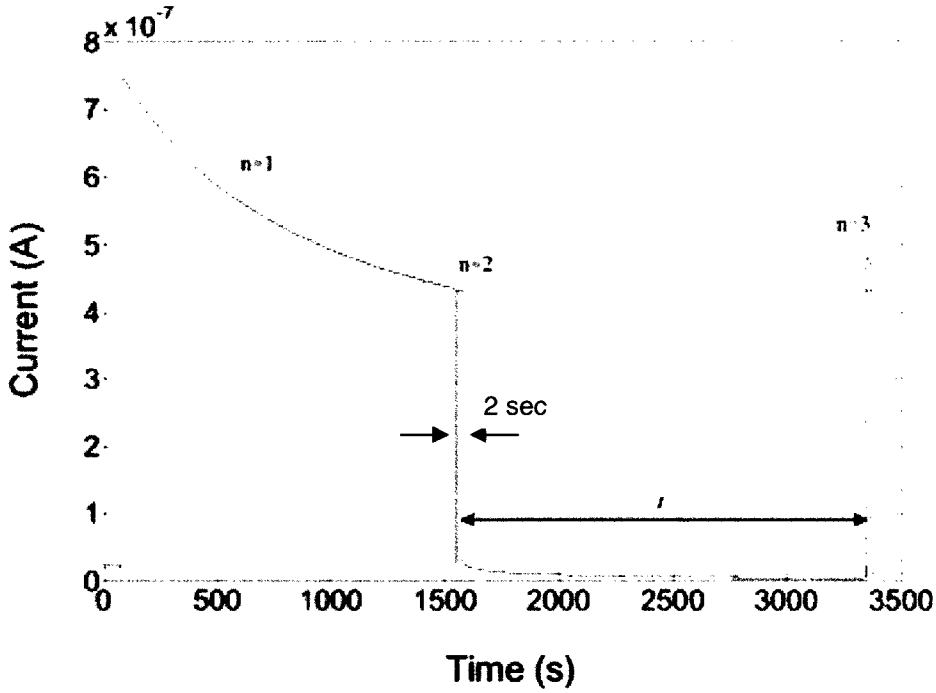

Figure 3.3. Raw signal from an a-Se detector used to determine sensitivity recovery for $t = 1800\ s$; $E = 4\ V/\mu m$, photon source = 75 *kVp* (*HVL* = 2.5 *mm* Al), $\dot{K} = 8.10\ cGy \cdot \text{min}^{-1}$.

3.3. X-ray sensitivity of an a-Se detector – non-biased case

3.3.1. Acquisition and Processing of Data

The experiment consisted of a sequence of short test measurements interleaved by long irradiation intervals, as depicted in Fig. 3.4. The test measurements were taken under constant bias by delivering a very small air-kerma to monitor the reduction in the detector signal. This drop in signal was due to the effects induced in the a-Se layer by the long irradiation (*fatiguing intervals*) delivered under no-bias conditions in between two subsequent test measurements. An ideal experiment would have been to take one measurement per day. In the first day, we would measure the initial sensitivity and in the subsequent days the residual sensitivity after delivering increased levels of air-kerma, under no-bias potential. This method would be very time consuming, therefore we opted for the first experimental sequence, acquired one per day.

In order to ensure the validity of our experiment, we evaluated the effect of the test measurements on the detector's sensitivity.

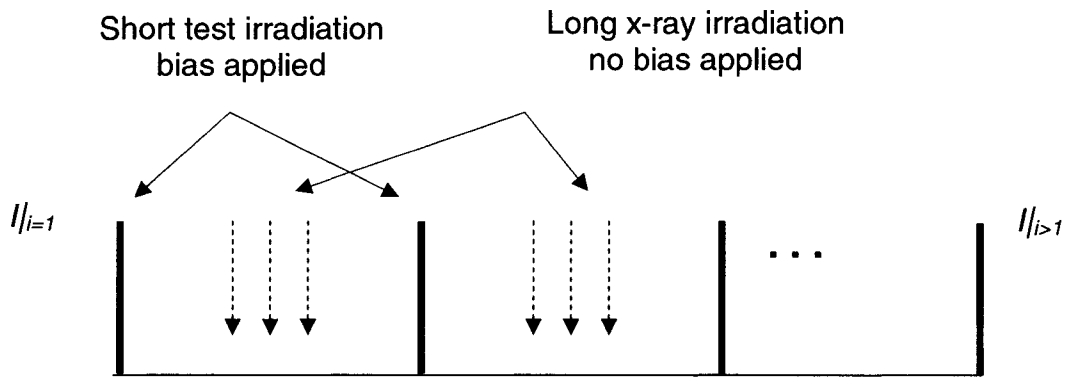

Figure 3.4. A typical experimental sequence showing test measurements alternated with long irradiation (fatiguing) intervals.

We found that the small amount of air-kerma (few cGy) delivered during these measurements did not affect the detector's sensitivity. The second test was to compare the effect of the fractionated delivery of air-kerma, i.e. sequence of test and long irradiation intervals, to the case of delivering the whole air-kerma at once. We found an agreement between the two in the order of 1%, therefore the sequence of test measurements does not influence the reduction in sensitivity effect.

We define $I|_{i=1}$ and $I|_i$ as the maximum collected currents corresponding to the first test measurement ($i=1$) and any test measurement ($i=1,2,...$) in the case of a multiple exposure experiment.. $I|_{i=1}$ is considered to be the initial photodetector response to radiation in the absence of any trapping-related effect.

The dark current of a detector built with blocking electrodes is mainly caused by thermal generation, and is not constant in time. The dark current was subsequently determined and subtracted from the raw signal of each test measurement by allowing a small waiting time interval (30 seconds) between the end of the long irradiation and the start of the immediately following test measurement.

The collected current was recorded during the test measurements for several air-kerma rates, x-ray photon energies and electric fields.

For the non-biased case, the detector's sensitivity corrected for dark current is similar to Eq. (3.1) and is given by

$$S_n = \frac{I|_i}{I|_{i=1}}, \text{ for } i \geq 1. \tag{3.3}$$

Sensitivity curves were generated from measured data using Eq. (3.3) as a function of delivered air-kerma and time for different air-kerma rates, applied electric fields and x-ray photon energies.

The measurements were performed in a light-free environment, as shown in Fig. 3.1. The detectors were stored with the electrodes short-circuited between any two complete experiments for 24 hours.

3.3.2. Acquisition and Processing of Data - Sensitivity Recovery

In order to determine the sensitivity recovery under conditions of no-bias, we performed the experimental sequence depicted in Fig. 3.5.

To quantify the recovery of sensitivity, the detector was initially subjected to a test measurement (under bias) to determine the initial current I_0. After this, the bias was removed and the detector was irradiated with a large air-kerma, i.e. 100 cGy. Test irradiation measurements were then repeated at 0, 5, 15, 30 minutes after the end of the long irradiation interval.

Dark current was subtracted from all collected current values. The measurements were made in a light-free environment. The percent recovery was then determined as follows

$$\% \text{ recovery} = \frac{I'_{t=0,5,15,30} - I'_{t=0}}{I_0 - I'_{t=0}} \times 100. \qquad (3.4)$$

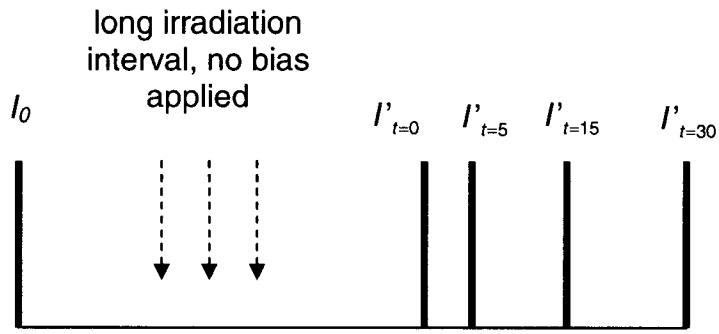

Figure 3.5. Experimental sequence used to determine the sensitivity recovery of a a-Se detector under no-bias conditions; $E = 4\ V/\mu m$, photon source = $75\ kVp$ ($HVL = 2.5\ mm$ Al), $\dot{K} = 8.10\ \text{cGy} \cdot \text{min}^{-1}$. I_0 is the initial current and I' recorded at $t = 0,5,15$ and 30 minutes after the fatiguing interval indicates the sensitivity recovery.

3.4 References

1. S. Steciw, T. Stanescu, S. Rathee, and B. G. Fallone, "Sensitivity Reduction in Biased Amorphous Selenium Photoconductors", J. Phys. D: Appl. Phys. 35, 1 (2002).

2. S. O. Kasap and J. A. Rowlands, CDROM: "Optoelectronics and Photonics: Principles and Practices" (Prentice Hall, 2000).

3. J. A. Rowlands, S. O. Kasap, "Amorphous Semiconductors Usher in Digital X-ray Imaging", Phys. Today 50 (11), 24-30 (1997).

Chapter 4:
Theoretical Considerations

In this chapter, a quantitative theory is developed to describe the mechanism of sensitivity reduction by considering that the photogenerated charge carriers can be captured in deep traps and become recombination centers for the subsequently generated opposite charge carriers.

A system of partial differential equations (PDEs) is introduced, and considered to describe the kinetics of electrons and holes in the amorphous selenium photoconductor layer. The initial and boundary conditions required to solve the kinetic equations are also presented.

An analytical solution for the total current density, defined as the sum of the conduction current density and the displacement current is derived.

4.1 Kinetic equations

The sensitivity of externally biased a-Se layers continuously decreases with accumulated air-kerma,[1-3] and has been shown in time-of-flight (TOF) experiments to be caused by deep entrapment levels.[4-7].

The mechanism of sensitivity reduction of selenium ERLs was theoretically described by Montrimas *et al*[2], Rakauskas *et al*[3] and Kalade *et al*[8]. These authors solved the kinetic equations characterizing selenium ERLs by

assuming that the photogenerated charge carriers can be captured in deep traps and may then recombine with subsequently-generated opposite charge carriers.

More recently, xerographic spectroscopy measurements, performed by Schiebel *et al*[6] to explain the sensitivity reduction and memory effects in selenium based x-ray detectors, support the mechanism described by the above authors. Kasap *et al*[5] used xerographic techniques based on the first residual potential and the cycled-up residual potential*, to explain the apparent increase in the capture coefficient by considering the recombination of holes with trapped electrons in the bulk, thus supporting the findings of references [2,3,8]. Zhao *et al*[9] experimentally studied the effect of bulk trapping of electrons on x-ray sensitivity in flat-panel x-ray detectors and indicated that the dominant mechanism is also given by recombination of the x-ray generated holes with trapped electrons. Kasap *et al*[10] analyzed TOF and interrupted field time-of-flight (IFTOF) measurements by considering the trapping and recombination mechanisms described by references [3,8], and showed that the recombination of drifting holes with trapped electrons follows the Langevin recombination.[11] In this case, the mechanism of Langevin recombination implies that a drifting charge carrier experiences a Coulombic capture field from a trapped opposite charge.

In xerographic experiments using an ERL detector (see Section 2.2), the induced trapping-related effects are investigated indirectly by monitoring the surface charge with a sample which is grounded at one end only. The resulting circuit is open, therefore the total current in the external circuit is zero. The x-ray sensitivity of ERLs is determined from the photo-discharge curves, and is defined on the basis of the decay rate of the surface potential. The kinetic equations of the photogenerated charge carriers inside the photodetector layer usually need to be solved for the first derivative of the applied potential.

However, for our case of a photodetector sandwiched between two metal parallel plate electrodes, and biased to a constant potential, the kinetic equations

---

* This xeroradiographic method refers to the photodischarge of the surface potential by a strongly absorbed light. By repeating the photoinduced discharge (PID) many times we obtain a cycled-up residual voltage measurement.

must to be solved for the total current density of both charge carriers, i.e. electrons and holes. We also have to consider a different set of initial and boundary conditions to describe the new configuration.

To explain the sensitivity reduction of parallel plate a-Se x-ray detectors, we considered a similar mechanism previously described by Montrimas *et al*[2]. Namely, we included the bulk space contribution from trapped charge carriers and considered that once trapped, the charge carriers can act as recombination centers for opposite free charges. Therefore, prior to any irradiation, the trapping centers are neutral,[6,12] and are then converted to attractive Coulombic centers by the capture of photogenerated carriers.

Sensitivity, or normalized collected current, is to be determined by solving a set of kinetic equations for the non-biased experimental sequence. Firstly, we determine the density of trapped electrons and holes corresponding to long irradiation intervals, when the bias is removed (see Appendix A3). The density of trapped charge carriers represents the cause of sensitivity reduction in the detector signal. Next step is to solve the kinetic equations under bias conditions for the total collected current at $t=0$, corresponding to each test measurement. The test measurements do not contribute to the reduction in sensitivity effect. Therefore, the sensitivity determined at $t=0$ for each test measurement, is given by the cumulative air-kerma delivered to the photodetector to that point in the experimental sequence. The density of trapped charge determined during the fatiguing intervals is inputted as initial condition for the trapped charge corresponding to each test measurement.

The time-dependant flow of photogenerated charge carriers in one dimension and in the presence of deep trapping sites will be considered. The detector sample is composed of a photoconducting selenium layer that is sandwiched between two plane parallel electrodes and externally biased to a constant potential to establish an electric field. During irradiation, x-ray photons are absorbed and generate charge carriers, i.e. electron-hole pairs, which can be collected on the electrodes through the applied field or can be lost in deep traps.

The dark current, which is measured in the absence of irradiation, depends on the applied electric field and temperature. This current must be as low as possible because it simply acts as a source of noise. Dark current has usually two main sources: thermal emission and carrier injection from the electrodes (i.e. injecting contacts). Our detector was built with blocking contacts to avoid the effect of injecting charge carriers from the electrodes and to minimize dark current.[13]

In our experiment, the main source of dark current was given by the carriers' generation from shallow traps. To isolate the cumulative effect of deep trapping on the detector sensitivity, we chose an appropriate sequence of measurements and then subtracted the dark current. This process is here described by solving the kinetic equations accordingly. Once irradiated, the a-Se layer must be isolated from irradiation (visible or ionizing) for approximately 24 hours before its sensitivity recovers completely to its initial level.[1] The release time of charge carriers from deep traps is therefore in the range of hours.[14]

The releasing time, i.e. the mean time of a captured charge carrier to be released from a trap, can be related to the energy of a deep state E_t by $t_r = \exp(E_t / kT)/\nu_0$, where $\nu_0 = 10^{12} s^{-1}$ is a phonon frequency, k the Boltzman constant, and T the temperature. The deep trapping sites for both electrons and holes are at $\sim 1\ eV$, which implies a release time of a few hours or longer. Based on the above considerations, we can safely assume that the carrier emission from deep traps is negligibly small during our experiment (i.e., in the range of minutes).

We define the coefficients that characterize the reduction in sensitivity mechanism as follows:

γ_{1n} and γ_{1h} are the capture coefficients for electrons and holes;

γ_{2n} and γ_{2h} are the recombination coefficients of electrons and holes with opposite trapped charge;

α is the generation rate of free electron-hole pairs;

M_1 and M_2 are the density of trapping sites for electrons and holes;

$m'_1(x',t')$ and $m'_2(x',t')$ are the density of trapped electrons and holes; and

$n(x',t')$ and $p(x',t')$ are the density of free electrons and holes,

where x' is the distance traveled by the incident radiation from surface within the a-Se layer and t' is the time.

The basic physical equations describing the kinetics of sensitivity reduction in the presence of an applied electric field are presented below.

The applied electric field is related to the space charge through Poisson's equation

$$\frac{\partial E'(x',t')}{\partial x'} = \frac{e}{\varepsilon}\left[m'_2(x',t') - m'_1(x',t') + p(x',t') - n(x',t')\right] \tag{4.1}$$

where E' is the applied electric field, e is the charge of the electron, $\varepsilon = \varepsilon_0\varepsilon_r$ is the permittivity of selenium.

The conduction current densities for electrons and holes are given by the sum of the drift and the diffusion currents as follows.[15]

$$J_n(x',t') = e\mu_n n(x',t')E'(x',t') + eD_n\frac{\partial n(x',t')}{\partial x'} \tag{4.2}$$

$$J_h(x',t') = e\mu_h p(x',t')E'(x',t') - eD_h\frac{\partial p(x',t')}{\partial x'} \tag{4.3}$$

where μ_n, μ_h and D_n, D_h are the mobilities and the diffusion constants of electrons and holes, respectively.

The total current density, $J(t')$ is the sum of the conduction current density, i.e. $J_c(x',t') = J_n(x',t') + J_h(x',t')$, and the displacement current

$$J(t') = J_c(x',t') + \varepsilon_0\varepsilon\frac{\partial E'(x',t')}{\partial t'}. \tag{4.4}$$

The next step in the process is based on the carrier dynamics. The rates at which the trapped charge carriers' concentrations change with time are given by the following set of equations[3]

$$\frac{\partial m'_2(x',t')}{\partial t'} = \gamma_{1h} p(x',t')\left[M_2 - m'_2(x',t')\right] - \gamma_{2n} n(x',t') m'_2(x',t') \tag{4.5}$$

$$\frac{\partial m'_1(x',t')}{\partial t'} = \gamma_{1n} n(x',t')\left[M_1 - m'_1(x',t')\right] - \gamma_{2h} p(x',t') m'_1(x',t') \tag{4.6}$$

The first term on the right of Eqs. (4.5) and (4.6) gives the rate of capture of mobile charge carriers into the available deep traps, and the second term gives the rate at which free carriers recombine with opposite trapped charge carriers.

Similarly as for the trapped charge carriers, we can define the rate at which free carriers' concentrations change[3]

$$\frac{\partial n(x',t')}{\partial t'} = \alpha_0 e^{-\mu x'} + \frac{1}{e}\frac{\partial J_n(x',t')}{\partial x'} - \gamma_{1n} n(x',t')\left[M_1 - m'_1(x',t')\right] - \gamma_{2n} n(x',t') m'_2(x',t') \tag{4.7}$$

$$\frac{\partial p(x',t')}{\partial t'} = \alpha_0 e^{-\mu x'} - \frac{1}{e}\frac{\partial J_h(x',t')}{\partial x'} - \gamma_{1h} p(x',t')\left[M_2 - m'_2(x',t')\right] - \gamma_{2h} p(x',t') m'_1(x',t') . \tag{4.8}$$

where α_0 is the photogeneration rate and is given by (see Appendix A.4)

$$\alpha_0 = \frac{5.45 \cdot 10^{13}}{W_{\pm}} \frac{\gamma_{Se}}{\gamma_0} \dot{K} \ (cm^{-3} s^{-1}) \tag{4.9}$$

μ is the linear attenuation coefficient of selenium, γ_0 and γ_{Se} are the mass energy absorption coefficients of air and selenium, and $\dot{K}$ is the air-kerma rate. In Eqs. (4.7) and (4.8), the first term represents the photogeneration rate, the second is given by the spatial variation of the collected current density, and the

third and the fourth are similar to the ones found in Eqs. (4.5) and (4.6), defining the trapping and recombination rates.

From Eqs. (4.5) - (4.8), the recombination of drifting electrons and holes with opposite trapped carriers is considered to follow the Langevin recombination mechanism.[11] Kasap *et al*[10] showed experimentally that this assumption is particularly valid for a-Se.

In general, we can also consider in Eqs. (4.5) - (4.8) an additional term to represent the release rate of electrons and holes from deep trapping sites. But as mentioned above, the release time of charge carriers from deep traps is in the order of hours, much longer than the timing considered, therefore these terms in Eqs. (4.5) - (4.8) can be safely dropped.

Another important aspect is that, in Eqs. (4.5) - (4.8), we do not make the assumption that the density of trapping sites is much larger that the density of trapped charge carriers[16,17], i.e. $M_1 >> m'_1(x',t')$ for electrons and $M_2 >> m'_2(x',t')$ for holes, so that we do not neglect the contribution given by the density of trapped carriers. In fact, the product of the density of free charge carriers with the trapped carriers makes the rate equations nonlinear.

The trapping and recombination mechanisms can also be described by considering the probability per unit time of each process $\gamma_i M_j = 1/T_i$, where i stands for any of the processes involved and $j = 1,2$, for each type of charge carrier[18].

To simplify Eqs. (4.5) - (4.8), we assume that $M_1 = M_2 = M_0 = const$, as suggested by the density of states diagrams of amorphous selenium.[19,20] During our experiments, we did not observed any radiation damage effect on the detector samples, therefore the density of deep traps should stay constant over time.

In our experiment, it is also assumed that the free volume charge in the layer is significantly less than the trapped charge, and therefore we can drop n, p, $\partial n/\partial t'$, and $\partial p/\partial t'$[8] from Eqs. (4.5) - (4.8). The diffusion of charge carriers is negligible compared with their drift, i.e. the externally applied potentials are far

greater than the thermal voltage ($\sim 25\ mV$). Therefore Eqs. (4.2) and (4.3) become

$$J_n(x',t') = e\mu_n n(x',t')E'(x',t') \tag{4.10}$$

$$J_h(x',t') = e\mu_h p(x',t')E'(x',t') \tag{4.11}$$

It is convenient to express Eqs. (4.4) – (4.8) in terms of the following dimensionless quantities as per J. Kalade *et al*[8]

$$x = \frac{x'}{l},\ t = \frac{t'}{t_0},\ \mathrm{j}_h = \frac{J_h}{j_0},\ \mathrm{j}_n = \frac{J_n}{j_0},\ \mathrm{j} = \frac{J}{j_0},\ E = \frac{E'}{E_0},\ m_i = \frac{m'_i}{M_0},\ i = 1,2 \tag{4.12}$$

with

$$E'(x',0) = E_0 = \sigma_0 / \varepsilon_0\varepsilon,\ \mathrm{J}_0 = \sigma_0 / t_0 \tag{4.12'}$$

where l is the a-Se layer thickness, σ_0 is the surface charge, t_0 is an arbitrarily chosen unit of time, J_0 is an arbitrarily defined initial current density, and E_0 is the applied electric field.

Using the assumptions stated above and the derivations from Appendix A.1, Eqs. (4.4) – (4.8) become

$$\frac{\partial E(x,t)}{\partial x} = a\left[m_2(x,t) - m_1(x,t)\right] \tag{4.13}$$

$$\frac{\partial m_2(x,t)}{\partial t} = \frac{j_h(x,t)}{E(x,t)}\Gamma_{1h}\left[1 - m_2(x,t)\right] - \frac{j_n(x,t)}{E(x,t)}\Gamma_{2n}m_2(x,t) \tag{4.14}$$

$$\frac{\partial m_1(x,t)}{\partial t} = \frac{j_n(x,t)}{E(x,t)}\Gamma_{1n}\left[1 - m_1(x,t)\right] - \frac{j_h(x,t)}{E(x,t)}\Gamma_{2h}m_1(x,t) \tag{4.15}$$

$$\frac{\partial j_n(x,t)}{\partial x} = -aQe^{-\eta x} + a\frac{j_n(x,t)}{E(x,t)}\left\{\Gamma_{1n}\left[1-m_1(x,t)\right]+\Gamma_{2h}m_2(x,t)\right\} \tag{4.16}$$

$$\frac{\partial j_h(x,t)}{\partial x} = aQe^{-\eta x} - a\frac{j_h(x,t)}{E(x,t)}\left\{\Gamma_{2h}m_1(x,t)+\Gamma_{1h}\left[1-m_2(x,t)\right]\right\} \tag{4.17}$$

$$j(t) = j_c(x,t)+\frac{\partial E(x,t)}{\partial t}. \tag{4.18}$$

where

$$a=\frac{elM_0}{\varepsilon_0\varepsilon E_0},\ Q=\frac{\alpha_0 t_0}{M_0},\ \Gamma_{1n}=\frac{\varepsilon_0\varepsilon\gamma_{1n}}{e\mu_n},\ \Gamma_{1h}=\frac{\varepsilon_0\varepsilon\gamma_{1h}}{e\mu_h},$$

$$\Gamma_{2n}=\frac{\varepsilon_0\varepsilon\gamma_{2n}}{e\mu_n},\ \Gamma_{2h}=\frac{\varepsilon_0\varepsilon\gamma_{2h}}{e\mu_h},\ \eta=\mu l \tag{4.19}$$

The general solution of Eqs. (4.13) – (4.18) can be written as a set of analytical functions of x and t as follows

$$E(x,t) = E_0(x)+tE_1(x)+\ldots$$

$$m_i(x,t) = m_{i0}(x)+tm_{i1}(x)+\ldots,\ i=1,2 \tag{4.20}$$

$$j_h(x,t) = j_{h0}(x)+tj_{h1}(x)+\ldots$$

$$j_n(x,t) = j_{n0}(x)+tj_{n1}(x)+\ldots$$

For this solution, the initial and boundary conditions are defined by

(a) The electric field intensity before the irradiation sequence is uniform throughout the photoconductor;

(b) The density of trapped carriers before each test measurement is given by the density of trapped carriers resulting from the irradiation during the long

intervals. It is assumed that there is no trapped charge before the first test measurement;

(c) The current densities of electrons and holes at any time during irradiation are zero at the electrodes, i.e. blocking electrodes, with the same polarity.

Therefore,

$$E(x,0) = 1,\ m_i(x,0) = m\ (i = 1,2),\ j_n(1,t) = 0,\ \ j_h(0,t) = 0 \tag{4.21}$$

where m is given by Eq. (a.3.15) in Appendix A.3. The parameter m, defined as the density of trapped charge carriers, was derived for the non-biased case, and it contains the dependence on air-kerma, air-kerma rate and effective x-ray energy.

From Eq. (20) and the boundary conditions (4.21), we obtain

$$E_0(x) = 1,\ j_{ni}(1) = 0,\ j_{hi}(0) = 0,\ i = 0,1,2,\ldots \tag{4.22}$$

To compare theory to experiment, the initial value of the total current density must correspond to the experimental test measurements, as a function of the density of trapped charge carriers, i.e., m, during the long irradiation intervals when the bias is turned off.

Experimentally, the total current is collected under constant potential between the sample electrodes; therefore we can define a boundary condition for the applied potential by

$$U(t) = \int_0^1 E(x,t)dx = const\,. \tag{4.23}$$

If we integrate Eq. (4.18) with respect to x, we obtain

$$j(t) = \int_0^1 j_c(x,t)dx + \frac{d}{dt}\left[\int_0^1 E(x,t)dx\right]. \tag{4.24}$$

Applying the boundary condition (4.23) to Eq. (4.24), the total current density is given by the following integral

$$j(t) = \int_0^1 j_c(x,t)dx. \tag{4.25}$$

We are interested in finding the initial total current density, i.e. $j(t=0) = j_0$. Therefore from Eqs. (4.20) and (4.25), we obtain

$$j_0 = \int_0^1 [j_{h0}(x) + j_{n0}(x)]dx. \tag{4.26}$$

Solving Eqs. (4.16) and (4.17) with Eq. (4.20), and considering the boundary conditions (4.21), we obtain $j_{h0}(x)$ and $j_{n0}(x)$ as follows

$$j_{h0}(x) = \frac{aQ}{(g_h - \eta)}\left(e^{-\eta x} - e^{-g_h x}\right) \tag{4.27}$$

$$j_{n0}(x) = \frac{aQ}{(\eta + g_n)}\left[e^{-\eta x} - e^{-(\eta+g_n)}e^{g_n x}\right] \tag{4.28}$$

where the coefficients involved are

$$\begin{aligned} g_h &= g_{h0}\left[1 + \left(\frac{\Gamma_{2n}}{\Gamma_{1n}} - 1\right)m\right] \\ g_n &= g_{n0}\left[1 + \left(\frac{\Gamma_{2h}}{\Gamma_{1h}} - 1\right)m\right] \end{aligned} \tag{4.29}$$

where

$$g_{h0} = \frac{\gamma_{1h} M_0}{\mu_h} \frac{l^2}{U},\ g_{n0} = \frac{\gamma_{1n} M_0}{\mu_n} \frac{l^2}{U}.$$

Replacing Eqs. (4.26) and (4.27) in Eq. (4.25) we obtain

$$j_0 = \frac{aQ}{(g_h - \eta)} \left[\frac{(1 - e^{-\eta})}{\eta} - \frac{(1 - e^{-g_h})}{g_h} \right] + \frac{aQ}{(\eta + g_n)} \left[\frac{(1 - e^{-\eta})}{\eta} + e^{-(\eta + g_n)} \frac{(1 - e^{g_n})}{g_n} \right]. \quad (4.30)$$

We now define the sensitivity similar to Eq. (3.3) of Section 3.3

$$S_n = \frac{j_0 |_i}{j_0 |_{i=1}}, \text{ for } i \geq 1 \quad (4.31)$$

where $j_0 |_{i=1}$ and $j_0 |_i$ are the total current densities corresponding to the first test measurement ($i = 1$) in the absence of any bulk space charge, and any test measurement ($i = 1,2,...$), respectively.

4.2 Comparison of Theory and Experiment

The reduction in x-ray sensitivity was calculated using Eq. (4.31) as a function of electric field, effective energy and a-Se layer thickness. A Monte Carlo method[21] was used to fit Eq. (4.31) to the experimental sensitivity curves obtained from Eq. (3.3). The fitting technique consists of random variation of the fitting parameters to minimize the sum of square of residuals, i.e. the difference between the observation and an estimated value of a function, in the least square method.

The fitting parameters used are as follows: g_{n0}, g_{h0} are given by Eq. (4.29) and characterize the capture coefficients of the excited electrons and holes, M_0 is given by the equation of φ in the Appendix A.3 and is defined as the density of deep traps, and ν, which is defined below, characterizes the recombination and trapping coefficient ratios of the charge carriers.

From Eq. (a.3.14) in Appendix A.3, we have

$$\varphi = \frac{2\alpha T_0}{KM_0}. \tag{4.32}$$

The other fitting parameter, ν, is given by Eq. (4.29) as follows

$$\nu = \frac{1}{2}\left(\frac{\Gamma_{2n}}{\Gamma_{1n}} - 1\right) = \frac{1}{2}\left(\frac{\Gamma_{2h}}{\Gamma_{1h}} - 1\right). \tag{4.33}$$

Detector sensitivities were theoretically determined for a variety of photodetector parameters and compared to the experimentally measured values.

4.3 References

1. S. Steciw, T. Stanescu, S. Rathee, and B. G. Fallone, "Sensitivity reduction in biased amorphous selenium photoconductors", J. Phys. D: Appl. Phys. **35**, 1 (2002).

2. J. Kalade, E. Montrimas and J. Rakauskas, "The Mechanism of Sensitivity Reduction in Selenium Layers Irradiated by X-Rays", Phys. Stat. Sol. A **25** 629 (1974).

3. J. Rakauskas, J. Kalade and E. Montrimas, "The Fatigue Mechanism of X-Irradiated Amorphous Se Layer ", Liet. Fiz. Rink. **12** 611 (1972).

4. C. Haugen and S. O. Kasap, "X-ray irradiation induced bulk space charge in stabilized a-Se x-ray photoconductors", J Appl. Phys. **84** 5495, (1998).

5. S. O. Kasap and V. Aiyah, "X-xay induced hole trapping in electroradiographic plates", J. Appl. Phys. **69**, 7087 (1991).

6. U. Schiebel, T. Buchkremer, G. Frings and P. Quadflieg, "Deep trapping and recombination in a-Se:As x-Ray sensitive photoreceptors" J. Non-Cryst. Sol. **115**, 216 (1989).

7. A. I. Kaminskas and I. Sidaravichus, "Physical and Technoogical Aspects of Electroradiography", Sci. Appl. Photo. **35** 624 (1994).

8. J. Kalade, E. Montrimas and J. Rakauskas, "Se Electroradiographic Layers Discharge Mechanism in Case of X-ray Irradiation", Liet. Fiz. Rink. **12** 597 (1972).

9. W. Zhao, G. DeCrescenzo, and J. A. Rowlands, "Investigation of lag and ghosting in amorphous selenium flat-panel X-ray detectors", Proc. SPIE **4682**, 9 (2002).

10. S. O. Kasap, B. Fogal, M. Z. Kabir, E. Johanson, and S. O'Leary, "Recombination of drifting holes with trapped electrons in stabilized a-Se photoconductors: Langevin Recombination", Appl. Phys. Lett. **84** 11 1991-1993 (2004).

11. P. Langevin, "Recombinaison et mobilités des ions dans les gaz," Ann. Chim. Phys. **28** 287-433 (1903).

12. M. Kastner and D. Adler, "Valence-Alternation Model for Localized Gap States in Lone-Pair Semiconductors", Phys. Rev. Lett. **37**, 1504 (1976).

13. A. Brauers, N. Conrads, G. Frings, U. Schiebel, M. J. Powell, and C. Glasse, "Charge Collection in a Se Photoconductor on a Thin Film Transistor Array During X-ray Imaging", Mat. Res. Soc.Symp. Proc. **467** 919-924 (1997).

14. M. Abkowitz and R. C. Enck, "Xerographic Spectroscopy of Localized Electronic States in Amorphous Semiconductors", Phys. Rev. B **25** 2567 (1982).

15. S. M. Sze, "Physics of Semiconductor Devices", 2nd edition, John Wiley & Sons Inc., 1981, pg. 51.

16. K. K. Kanazawa and I.P. Batra, "Deep-Trapping Kinematics", J. Appl. Phys. **43** 4, 1845-53 (1972).

17. I.P. Batra, K.K. Kanazawa and H. Seki, "Discharge Characteristics of Photoconducting Insulators", J. Appl. Phys. **43** 4, 1845-53 (1972).

18. S. O. Kasap, V. Aiyah, B. Polischiuk, A. Bhattacharyya, and Z. Liang, "Deep-trapping kinematics of charge carriers in amorphous semiconductors: A theoretical and experimental study", Phys. Rev. B **43** 8, 6691-6705 (1991).

19. M. Abkowitz, "Density of states in a-Se from combined analysis of xerographic potentials and transient transport data," Philos. Mag. Lett. **58** (1), 53-57 (1988).

20. H.-Z. Song, G. J. Adriaenssens, E. V. Emelianova, and V. I. Arkhipov, "Distribution of gap states in amorphous delenium thin films", Phys. Rev. B **59** (1999) 10610.

21. P. Stavrev, A. Niemierko, N. Stavreva, and M. Goitein, "The Application of Biological Models to Clinical Data", Physica Medica **17** (2001).

Chapter 5: Results and Discussion

In this chapter, the experimental results for the x-ray sensitivity response of a-Se parallel plate detectors are presented for different operating conditions, such as air-kerma rates, applied electric fields, and x-ray effective energies. The sensitivity was measured for both the biased and non-biased cases. The biased case refers to the condition when a potential is continuously applied across the photodetector's layer during time of the experiment. The non-biased case is described by a sequence in which the detector is kept unbiased during fatiguing irradiation intervals, and biased for sensitivity probing with short irradiation pulses. The sensitivity recovery was also measured.

Predicted and experimental dependences of the sensitivity upon the air-kerma, applied electric field, and x-ray effective energy are presented for the non-biased case. Sensitivity versus photodetector thickness profiles are theoretically derived for several x-ray effective photon energies. The theoretically-determined density of traps responsible for the reduction in sensitivity process, as well as, the numerical determined values of the trapping and recombination is also presented.

5.1. Comparison of the biased and non-biased case

5.1.1. Maximum detector signal for bias case

The initial current $I'_{max}|_{i=1}$ was measured for different applied electric fields (Fig. 5.1) and air-kerma rates (Fig. 5.2). Each data point in these graphs was obtained after the detector was left un-irradiated and in the dark for 24 hours to insure that the sensitivity had completely recovered between measurements.

In the absence of any bulk-space charge, the a-Se detector response to irradiation varies linearly with the air-kerma rate and the applied electric field. For a given value of the applied electric field and the x-ray effective photon energy, the detector's signal increases with air-kerma rate because the production rate of electron-hole pairs is proportional to the energy deposited in the photodetector layer.

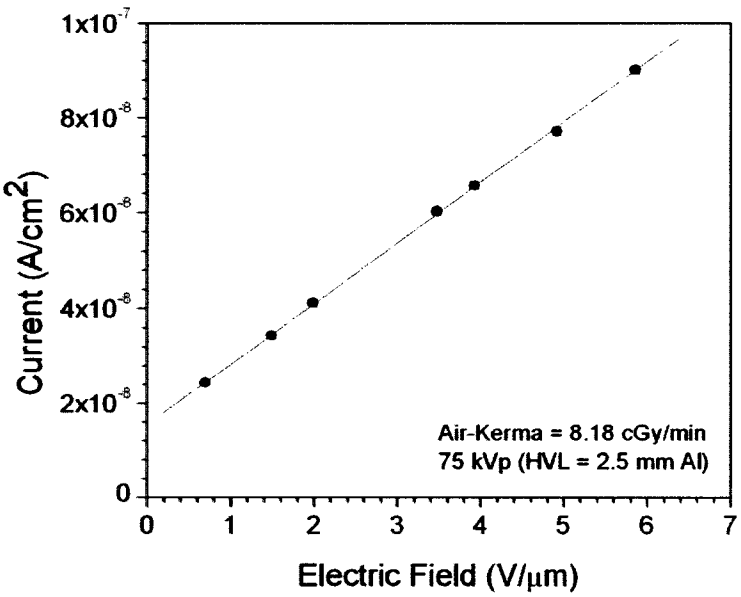

Figure 5.1. Maximum detector signal versus applied electric field; air-kerma rate $\dot{K} = 8.18\ cGy/\text{min}$, x-ray photon source = 75 kVp (HVL = 2.5 mm Al), a-Se layer thickness is $239\mu m$.

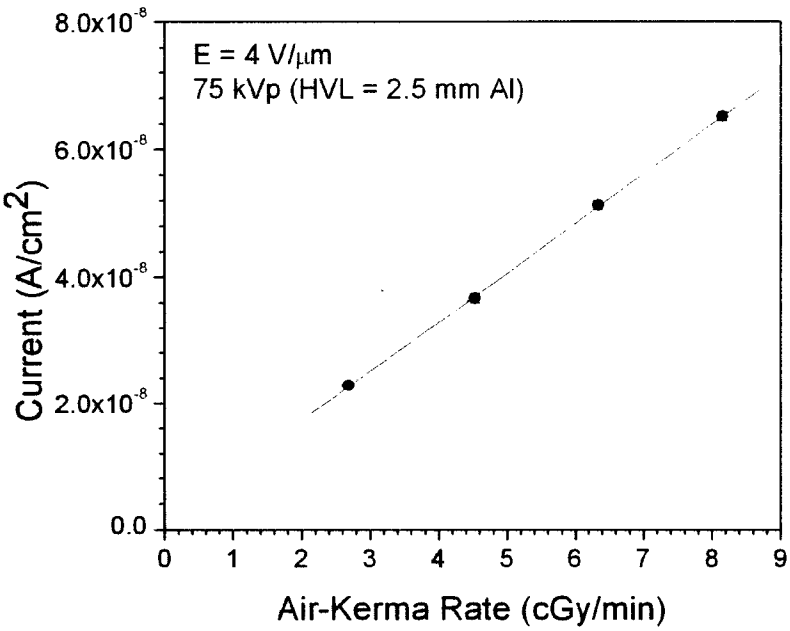

Figure 5.2. Maximum detector signal versus air-kerma rate; $E = 4\ V/\mu m$, x-ray photon source = 75 kVp ($HVL = 2.5\ mm$ Al), a-Se layer thickness is $239\mu m$.

The signal also increases with electric field because the rate of charge-carriers general recombination decreases resulting in the increased collection of charge. For both Fig. 5.1 and Fig. 5.2, the size of the error bars is comparable to the size of the symbols.

5.1.2. Sensitivity curves – air-kerma rate dependence

Several sensitivity curves were generated for a variety of different air-kerma rates for both biased and non-biased cases. Air-kerma rates were adjusted experimentally by varying the source-to-detector-distance (SDD). The detector sensitivity drops substantially as the air-kerma delivered to the detector increases, as shown in Figs. 5.3 and 5.4.

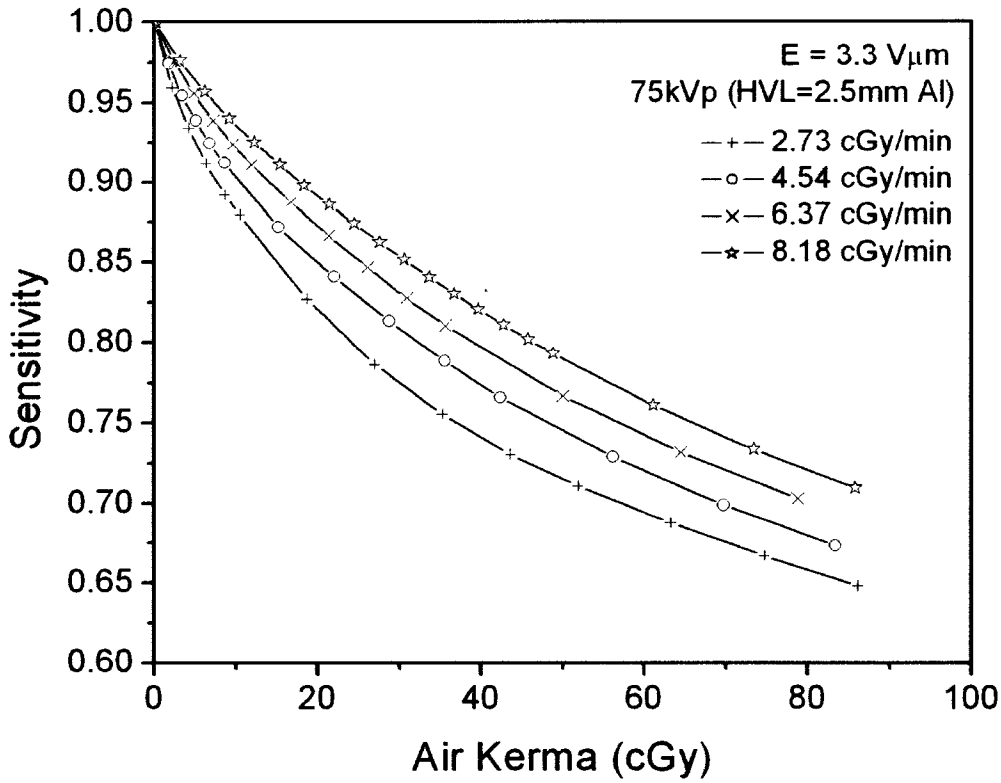

Figure 5.3. Sensitivity dependence of a-Se layer versus air-kerma for several air-kerma rates, corresponding to the biased case; $E = 3.3\ V/\mu m$, photon source = 75 kVp (HVL = 2.5 mm Al), a-Se layer thickness is $239\mu m$.

For the biased case, i.e., Fig. 5.3, after delivering approximately 90 cGy of air-kerma, the detector sensitivity drops by roughly one third of its initial value. The sensitivity curves are the result of competing rates between the charge-carriers photogeneration, their trapping and recombination mechanisms within the a-Se photodetector layer.

It is also evident from Fig. 5.3 that the detector sensitivity depends on the delivered air-kerma rate. For the same value of the air-kerma delivered to a-Se, low air-kerma rates produce lower detector sensitivity than higher air-kerma rates.

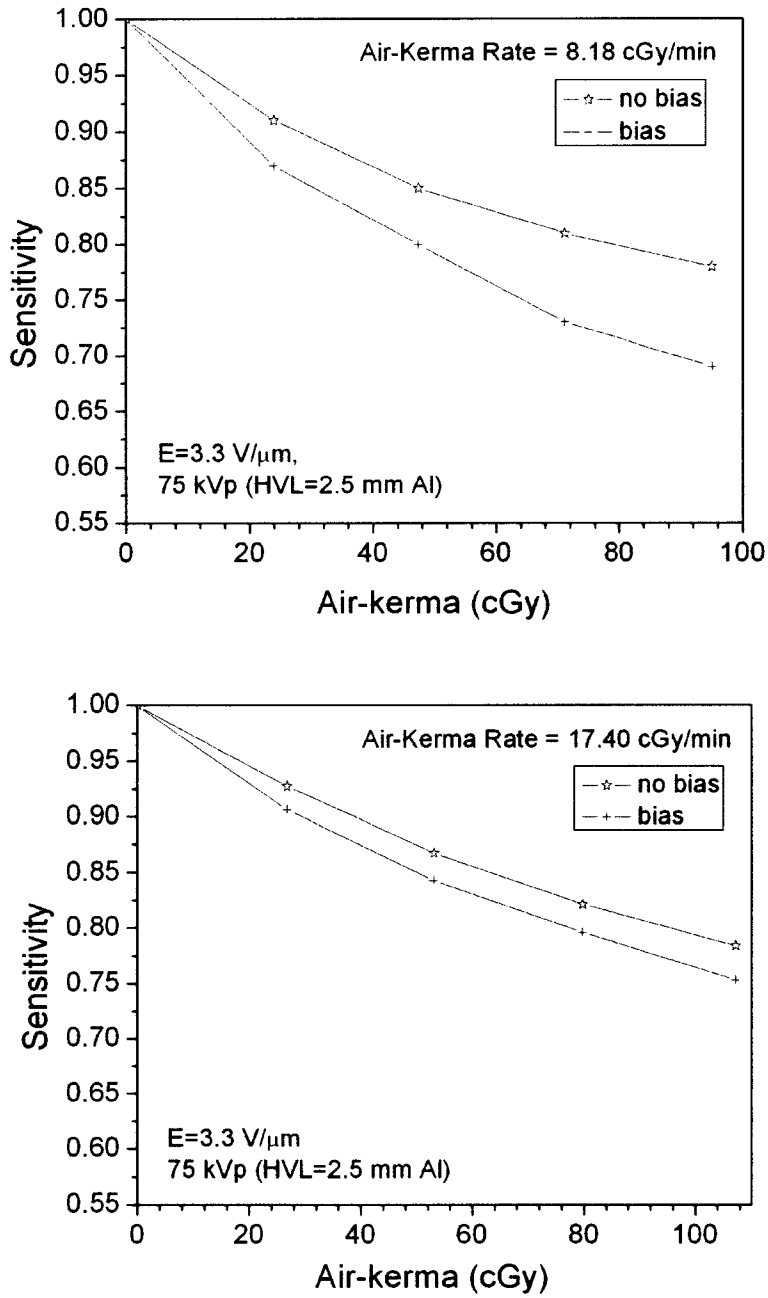

Figure 5.4. Detector sensitivity versus air-kerma for 8.18 and 17.40 cGy/min air-kerma rates, corresponding to both biased and unbiased cases; $E = 3.3\ V/\mu m$, photon source = 75 kVp (HVL = 2.5 mm Al), a-Se layer thickness is $239\mu m$.

This occurs because the occupation of deep traps is greater for lower air-kerma rates. Experiments with ERLs have shown that this phenomenon is due to differences in the charge carriers' lifetimes with respect to the trapped-carriers lifetimes, which are responsible for the reduction in detector sensitivity[1].

In Fig. 5.4 a similar trend can also be observed for the non-biased case. Comparing the non-biased and the biased case, the latter shows a higher sensitivity reduction effect (Fig. 5.4). This is due to the presence of the electric field during the fatiguing irradiation intervals. In the biased case the collection efficiency is higher than in the non-biased case, resulting in a higher density of empty traps available to be filled in.

5.1.3. Sensitivity curves – electric field dependence

The magnitude of the sensitivity reduction is substantially influenced by the applied electric field, which is essential to the collection of the photogenerated carriers. Since electron-hole recombination is dependant on the externally applied electric field, the collection efficiency of photogeneration electrons and holes in a-Se is also affected by the electric field.

Recombination models including geminate[2] and columnar[3] recombination, and a more recent approach based on Monte Carlo simulations,[4] show that as the applied field increases, the parameter $W_{\pm}$, which is the energy required to generate a detectable electron-hole pair, decreases, and therefore the collection of charge carriers becomes more efficient. The perturbation of the applied electric field due to bulk space charging or external effects will greatly alter the detector's response.

It was shown in Fig. 5.1 that, when bulk space charging effects are neglected, there is a linear relationship between the amount of carriers collected and the strength of the applied electric field. Evidence of this is shown in Fig 5.5, where detector sensitivities were measured for several different applied electric field strengths and delivered air-kerma.

Increasing the strength of the applied electric field the collection efficiency is also increased, due to a stronger interaction of charge carriers with the applied electric field. There are less electrons and holes available to fall under trapping-related effects. Therefore, the sensitivity increases with the increase in the applied electric field strength. Higher electric fields can also pull loosely bound charge from shallow traps more easily than lower electric fields.

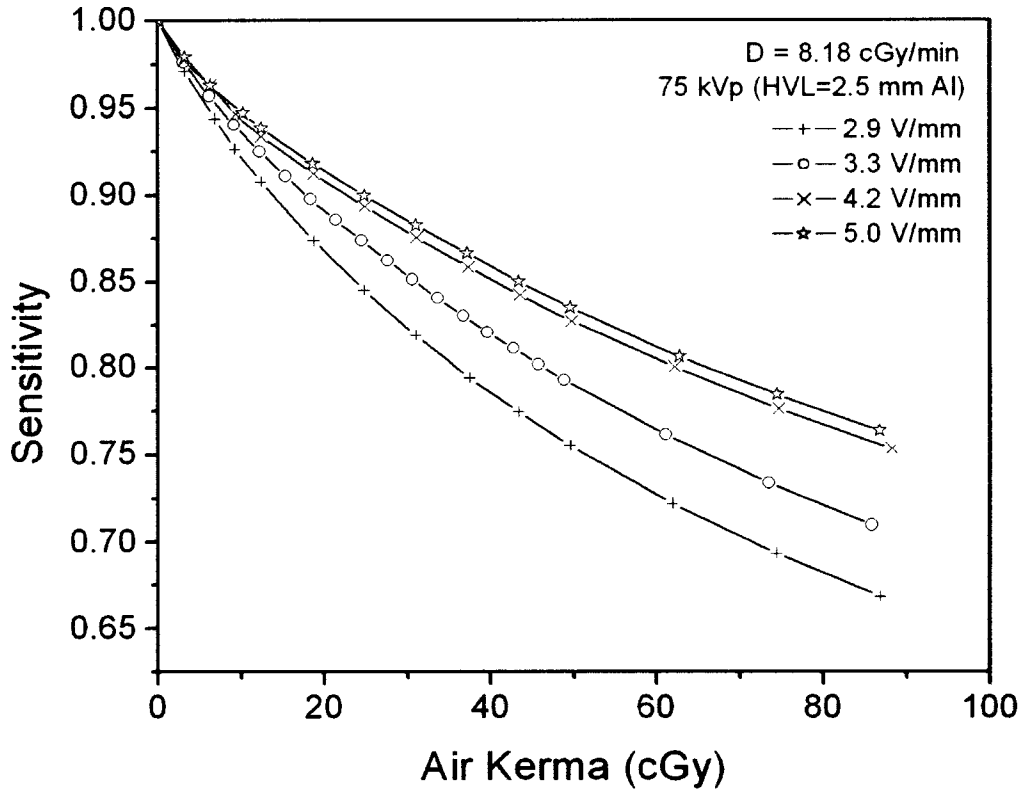

Figure 5.5. Sensitivity dependence versus air-kerma for several applied electric fields, corresponding to the biased case; air-kerma rate $\dot{K} = 8.10\ \text{cGy} \cdot \text{min}^{-1}$, x-ray photon source = 75 kVp (HVL=2.5 mm Al), a-Se layer thickness is $239 \mu m$.

As a result, there is a much greater trapping cross-section for both electrons and holes at lower applied electric fields.

A similar trend, shown in Fig. 5.6, was observed for the non-biased case. The reduction in sensitivity effect is less intense for the non-biased case compared to the case when the detector was continuously biased during irradiation.

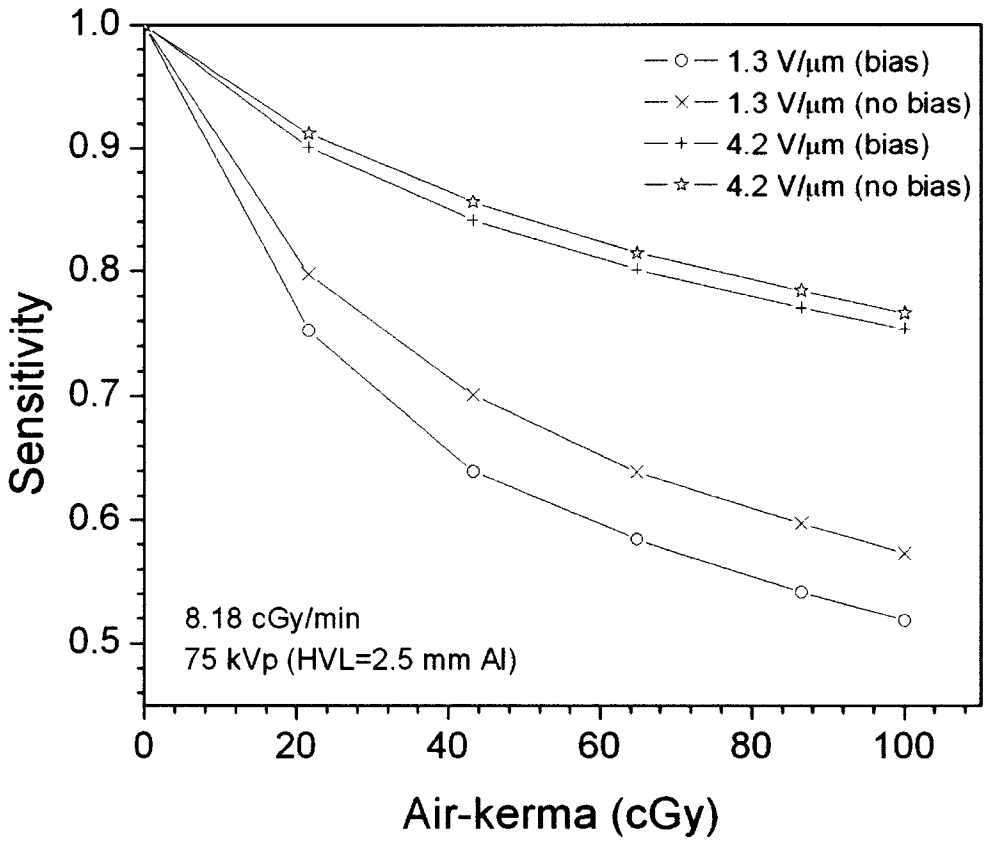

Figure 5.6. Sensitivity vs. air-kerma for several applied electric fields, corresponding to both bias and non-biased cases; air-kerma rate $\dot{K} = 8.10\ \text{cGy} \cdot \text{min}^{-1}$, x-ray photon source = 75 kVp (HVL=2.5 mm Al), a-Se layer thickness is $239 \mu m$.

5.1.4. Sensitivity curves – effective energy dependence

The reduction of sensitivity during irradiation is strongly influenced by the physical location of the photo-generated carriers in the a-Se layer. Figure 5.7 illustrates, for the biased and non-biased cases, the changes in sensitivity for different effective photon energies.

The attenuation coefficient of a-Se varies with different effective energies resulting in a variation of the air-kerma deposited in the photodetector layer. In order to obtain the same initial detector signal $I'_{\max}\big|_{n=1}$ for each energy, the air-kerma rate in a-Se ($\dot{K}_{Se}$) was adjusted by varying the source-to-detector-distance (SDD).

The decrease in sensitivity was larger for greater effective photon energies. The air-kerma rates for a-Se in these experiments do vary slightly between the different energies (increases by approximately 9 % from 133.3 KeV to 30.9 KeV) because $W_{\pm}$ varies with energy [3]. However, the main effect exhibited in Fig. 5.7 is due to differences in effective photon energies.

When the detector is irradiated by low energy x-rays, most of the carriers are produced at the surface of the detector since the half-value layer of a-Se for 30 keV photons is $\sim 100\mu m$. The top electrode, facing the x-ray source, is positively biased; therefore the electrons are readily collected.

Since holes have *Schubwegs* that are roughly 10 times greater than those of electrons[6], they are not as readily trapped and can be collected on the negatively-biased electrode after traveling through the thickness of the photodetector. Because of the short distance that the electrons have to travel in order to be collected, fewer are captured by trap centers and the rate of bulk space charging is kept low.

When high energy x-rays strike the top electrode, there is a fairly homogeneous distribution of photogenerated carriers in the a-Se bulk. As a result, on average, the electrons have to travel much further to reach the positive

electrode, and therefore are more prone to being trapped. A higher rate of bulk space charging occurs, and the detector's sensitivity is reduced to a larger extent.

Figure 5.7 shows that the sensitivity reduction for the non-biased case is lower than for the biased case.

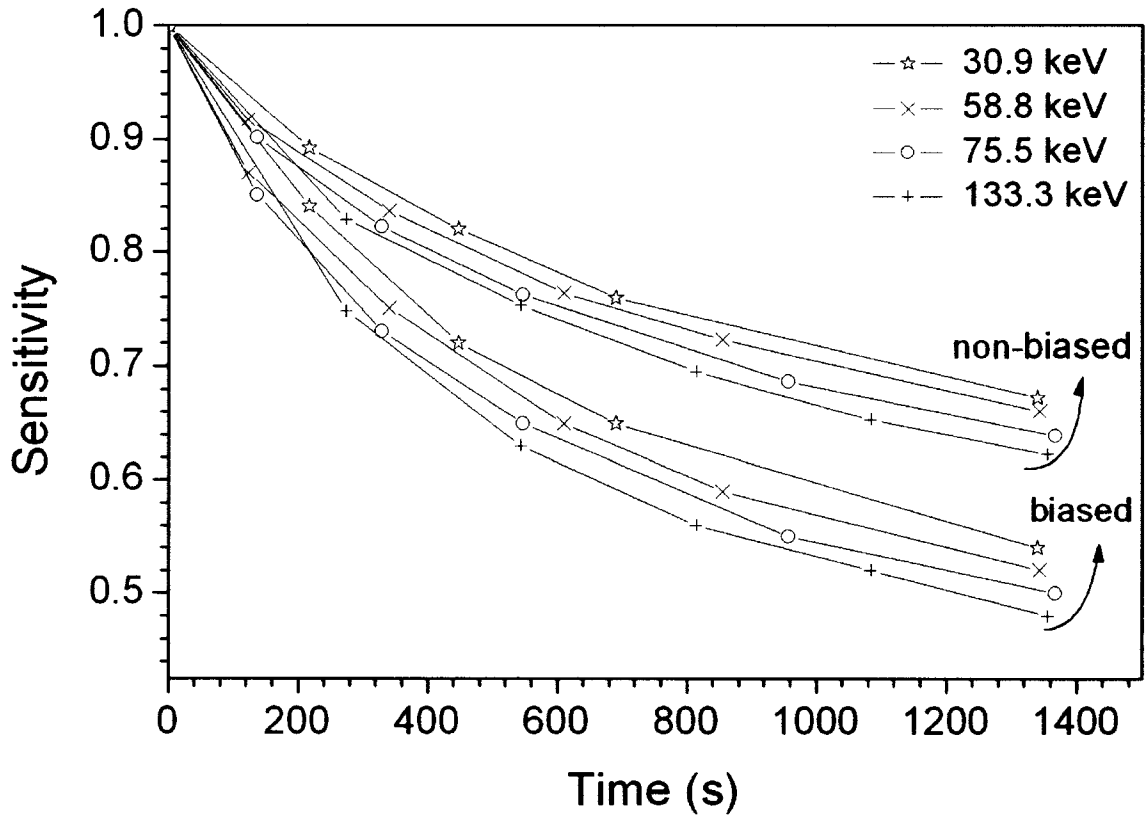

Figure 5.7. Detector sensitivity versus irradiation time, for the same initial value of collected current, I_0, but for several different effective photon energies, $E = 1.7\ V/\mu m$.

5.1.5. Sensitivity curves – recovery

The percentage recovery for a variety of recovery times, i.e., 5, 15 and 30 minutes, was measured post irradiation for an a-Se detector to 100 cGy and 200 cGy (Fig. 5.8). The mechanism of sensitivity recovery consists in the release of charge carriers, i.e. electrons and holes, from deep trapping sites.

The recovery curves were obtained for both cases, under bias and no-bias conditions.

The majority of the sensitivity gain from short recovery times is from released holes, since the electrons are more deeply trapped than the holes, and therefore are released slower.[7] As the charge carriers are thermally released, the bulk space becomes less charged and the sensitivity of the detector increases with time.

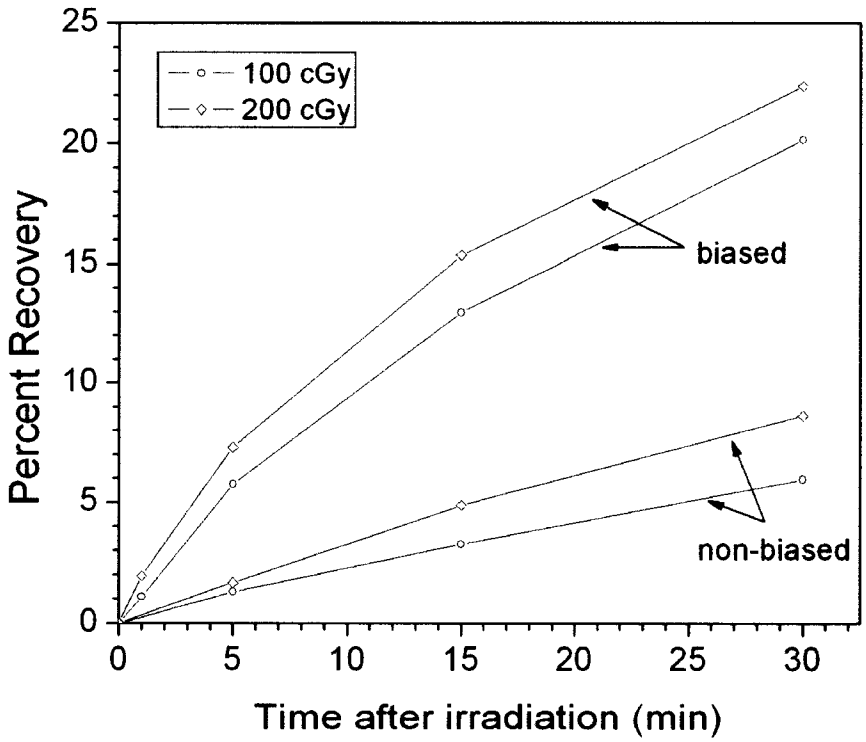

Figure 5.8. Percent recovery of the detector's sensitivity, compared to the initial sensitivity after receiving 100 cGy and 200 cGy.

Since the occupation of trapping sites increases with the level of air-kerma delivered, it is expected that the initial release rate of charge carriers post-irradiation would increase with dose as well. This is indeed the case shown in Fig. 5.8. The sensitivity recovers faster for a detector irradiated to a large air-kerma than one which was irradiated to a smaller air-kerma. However, the total time of recovery will be longer for the detector that received the larger air-kerma because it has to recover from a lower sensitivity level.

After we stopped the irradiation, the sensitivity recovery is negligibly small in the first seconds because few electrons and holes are released from deep traps. In the non-biased case, the sensitivity recovery is slower than in the biased case.

5.2. Theoretical fitting of the data for the non-biased case

The theoretical results are compared to the experimental data for the non-biased case for different operating conditions. All the experimental curves are fitted with the following best fitting parameters: $g_n = 301.7$, $g_p = 1685$, $M_0 = 0.85 \cdot 10^{13}\ cm^{-3}$ and $\nu = 2.266$.

The dependence of sensitivity on delivered air-kerma during long irradiation intervals and without-bias for different electric field strengths applied during test measurements is shown in Fig. 5.9. The detector sensitivity drops substantially with an increase in air-kerma. This is due to the increase in the concentration of trapping centers for electrons and holes with increasing air-kerma.

The magnitude of the sensitivity reduction is substantially influenced by the applied electric field during test measurements. The collection efficiency increases with the increasing strength of the applied electric field, suggesting a decrease in the recombination rate of the free carriers with the trapped ones of opposite charge.

As previously mentioned, the detector signal is influenced by the location of the photo-generated charge carriers in the photodetector layer. The location of charge-carriers is determined mainly by the energy of the photons. Figure 5.10 shows the theoretical results compared to experiment data for different x-ray effective photon energies.

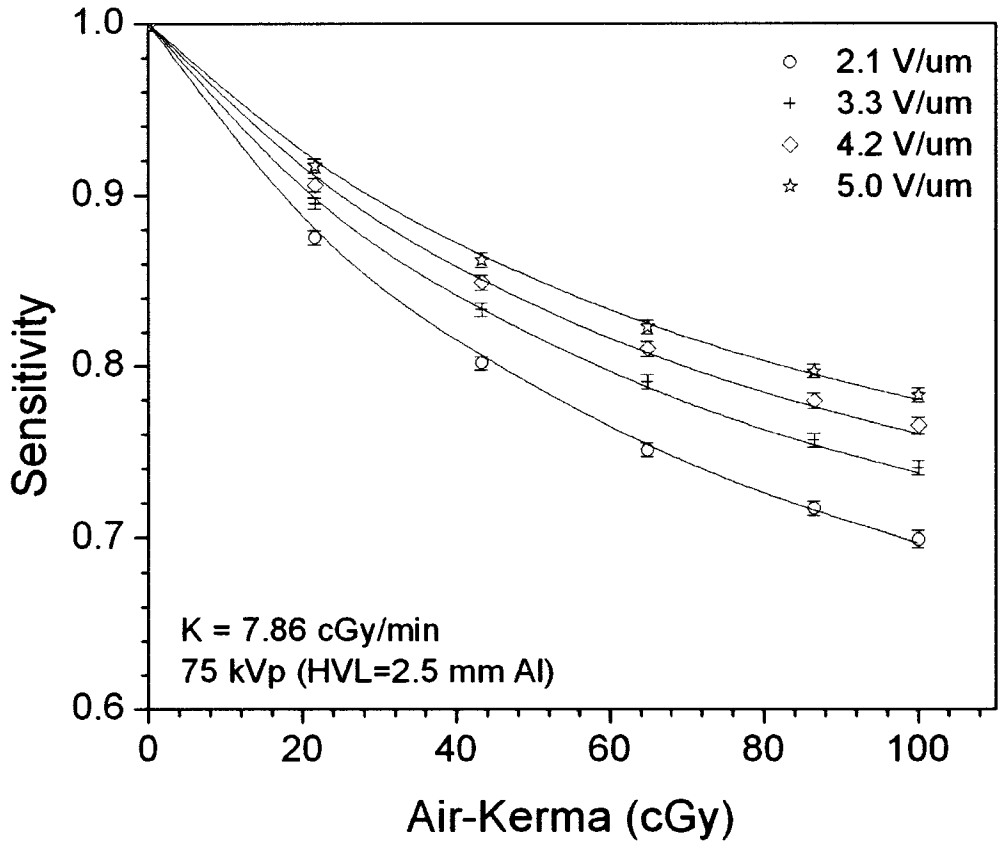

Figure 5.9. Sensitivity dependence of a-Se layer versus air-kerma for several electric fields applied during test measurements; $\dot{K} = 7.86$ cGy/min, photon source $= 75$ kVp (HVL $= 2.5$ *mm* Al), a-Se layer thickness is 239 μm. The theoretical results are shown as lines and the experimental data is depicted as scattered points. Solid lines were calculated using Eq. (4.31) with $g_n = 301.7$, $g_p = 1685$, $M_0 = 0.85 \cdot 10^{13}\ cm^{-3}$ and $\nu = 2.266$.

The sensitivity reduction is larger for greater values of the x-ray effective energy. For low effective energies most of the charge carriers, i.e. electron hole pairs, are generated near the photodetector surface, and for greater effective energies, the distribution of electron-hole pairs becomes more uniform. Due to different *Schubwegs* for electrons and holes, the electrons have to travel on a longer path in the photodetector layer. They are, therefore, more likely to be trapped and recombine in the photoconductor layer.

Tables 1 and 2 show the χ^2 values representing the goodness-of-fit for each sensitivity curve plotted in Figs. 5.9 and 5.10. All χ^2 values were calculated using a sensitivity error of $\pm 1\%$.

Electric field ($V/\mu m$)	χ^2	Degrees of freedom
2.1	1.44	6
3.3	0.69	6
4.2	0.95	6
5	1.20	6

Table 1. Goodness-of-fit for sensitivity curves corresponding to several applied electric fields

Effective energy (keV)	χ^2	Degrees of freedom
133.3	2.95	6
75.5	1.19	6
58.8	1.03	6
30.9	1.54	6

Table 2. Goodness-of-fit for sensitivity curves corresponding to several x-ray effective energies.

Figure 5.11 shows the initial sensitivity dependence on the a-Se layer thickness for several x-ray effective photon energies. The sensitivity profiles are determined from Eq. (4.31) using the same values of the fitting parameters used in Figs. 5.9 and 5.10, i.e. $g_n = 301.7$, $g_p = 1685$, $M_0 = 0.85 \cdot 10^{13}\ cm^{-3}$ and $\nu = 2.266$.

As expected, the sensitivity peak is shifted to higher thickness values with the increase of the x-ray effective energy. Our predictions are in good agreement with the theoretical and experimental results from ERLs.[1,8]

The complex dependence of the sensitivity on the photodetector layer thickness and the x-ray effective energy is determined by the competing effect of the amount of energy absorbed in the layer and the decrease in the collection efficiency due to trapping.

For a low effective energy and a constant electric field applied across the photodetector, by increasing the layer thickness, more energy is deposited, which results in an increase in the collection efficiency, or sensitivity. Increasing the thickness beyond the optimal value for which the maximum sensitivity is reached, i.e. sensitivity peak, the collection efficiency of charge carriers decreases due to limited Schuwbegs. The electrons and holes have to travel a longer path in the photodetector layer therefore they become more likely to be trapped. For higher effective energies the sensitivity peak is broader than for low energies, due to a more uniform distribution of charges in the photodetector layer.

From Fig. 5.11, one can determine the optimal thickness required for a particular range of x-ray energies. The shape of the initial sensitivity profiles and the position of the sensitivity peaks may vary with the intrinsic properties of different a-Se photoconductor layers and the particular dopping impurities used.

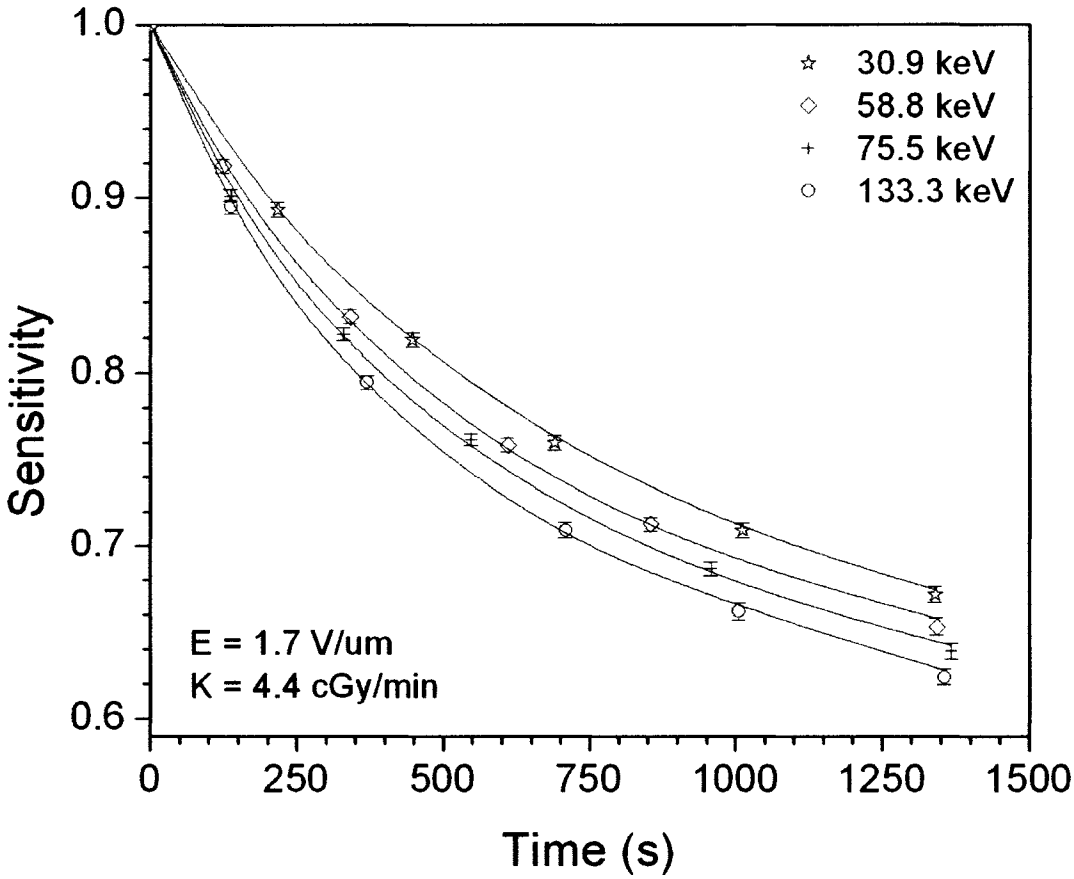

Figure 5.10. Sensitivity versus irradiation time for the same initial sensitivity values, but for several different effective photon energies; $\dot{K} = 4.4$ cGy/min, $E = 1.7$ V/μm, a-Se layer thickness is 239 μm. The theoretical results are shown as lines and the experimental data is depicted as scattered points. Solid lines were calculated using Eq. (4.31) with $g_n = 301.7$, $g_p = 1685$, $M_0 = 0.85 \cdot 10^{13}$ cm^{-3} and $\nu = 2.266$.

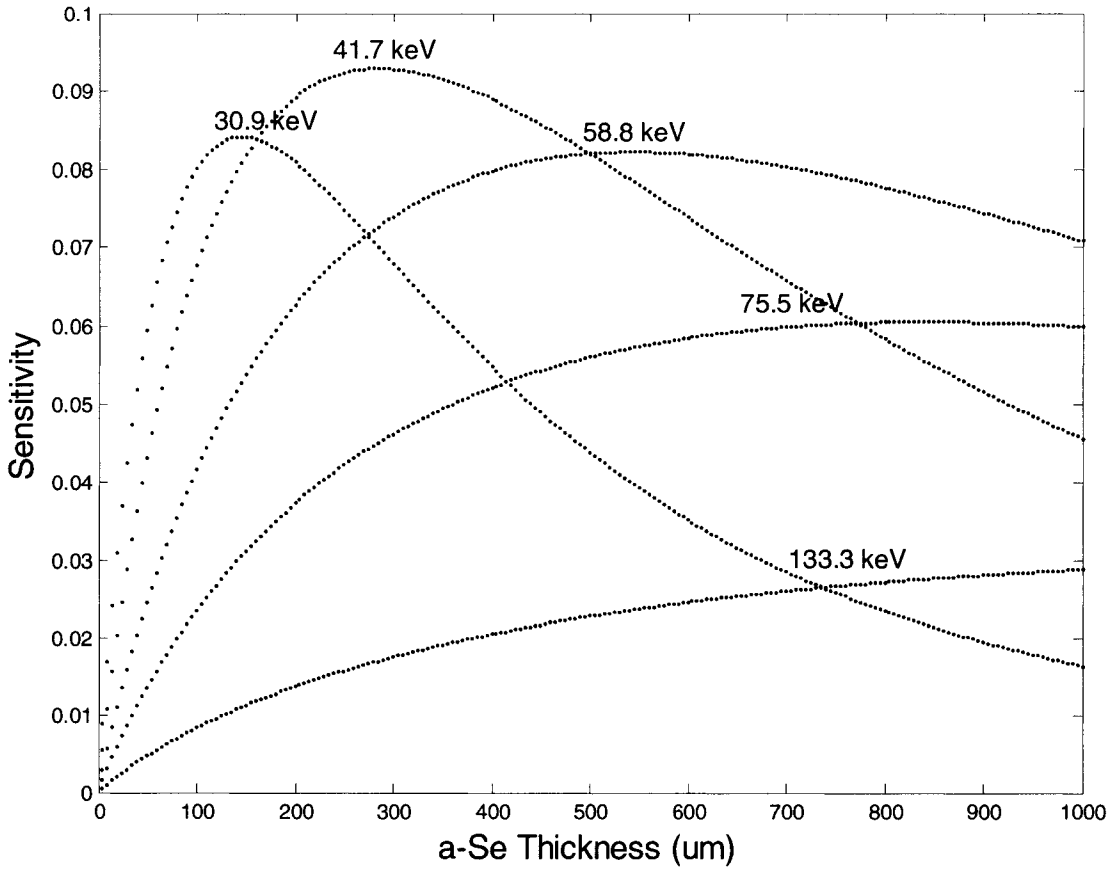

Figure 5.11. Initial sensitivity versus a-Se layer thickness for different effective photon energies; $\dot{K} = 4.4$ cGy/min, $E = 4.2$ V/μm, a-Se layer thickness is 239 μm. The lines were calculated using Eq. (4.31) with $g_n = 301.7$, $g_p = 1685$, $M_0 = 0.85 \cdot 10^{13}$ cm^{-3} and $\nu = 2.266$.

5.3. Trapping and recombination cross-sections for electrons and holes

From the experimental and calculated results of the sensitivity reduction in a-Se photoconductor layer, one can determine the cross-sections of trapping and recombination processes. The density of the deep trapping sites for a certain photodetector layer was determined as a fitting parameter in Eq. (4.31), and its value was found to be $M_0 = 0.85 \cdot 10^{13}\ cm^{-3}$, as already noted.

The trapping coefficients can be determined from Eq. (4.29) as follows

$$\gamma_{1n} = \frac{g_{n0}\mu_n U}{M_0 l^2},\ \gamma_{1h} = \frac{g_{h0}\mu_h U}{M_0 l^2} \tag{5.1}$$

and their values are $\gamma_{1n} = 1.48 \cdot 10^{-10}\ cm^3/s$ and $\gamma_{1h} = 4.42 \cdot 10^{-8}\ cm^3/s$ for electrons and holes, respectively.

From Eq. (4.33), it follows that the relationship between the capture and recombination probabilities of the electrons and holes in the presence of an electric field is given by

$$\gamma_{2h} = \gamma_{2n}\frac{\gamma_{1h}}{\gamma_{1n}} \tag{5.2}$$

The recombination coefficients are determined from Eq. (4.33) as follows

$$\gamma_{2n} = (2\nu + 1)\gamma_{1n},\ \gamma_{2h} = (2\nu + 1)\gamma_{1h} \tag{5.3}$$

The values of the recombination coefficients are $\gamma_{2n} = 0.82 \cdot 10^{-9}\ cm^3/s$ and $\gamma_{2h} = 2.45 \cdot 10^{-7}\ cm^3/s$ for electrons and holes, respectively. Because the thermal velocity of the carriers is $v_t = 10^7 cm/s$, the cross-sections for capture and recombination processes can be determined and are shown in Table 1.

In Table 1, the cross-sections' values of capture and recombination processes are compared with similar data published in the literature. Differences between our values and those of others may be accounted for by substantial differences in a-Se materials were used.

The type and fraction of doping impurities were not reported for the data given in Table 3 from Montrimas *et al*[8] and Rakauskas *et al*[1]. It is known that very small amounts of impurities can have a pronounced effect upon the behavior of a-Se layers.[9]

The electron range can be increased and the hole range decreased by suitable doping of a-Se with certain impurities.[12] Experimentally, it was found that a 0.2% – 1% arsenic (As) addition to a-Se is sufficient to reduce its crystallization rate.

	σ_{1n} (cm^2)	σ_{1h} (cm^2)	σ_{2n} (cm^2)	σ_{2h} (cm^2)
Montrimas *et al*[8]	$(0.1-1.0)\cdot10^{-17}$	$(0.2-1.0)\cdot10^{-15}$	$(0.5-1.8)\cdot10^{-16}$	$(0.8-1.6)\cdot10^{-14}$
Rakauskas *et al*[1]	$1.25\cdot10^{-17}$	$1.20\cdot10^{-15}$	$1.62\cdot10^{-16}$	$1.55\cdot10^{-14}$
Schiebel et al[10]	$\sim10^{-16}$	$\sim10^{-16}$	$5.00\cdot10^{-15}$	$0.90\cdot10^{-14}$
Kasap *et al*[11]	-	-	-	$0.36\cdot10^{-14}$
Present Work	$1.48\cdot10^{-17}$	$4.42\cdot10^{-15}$	$0.82\cdot10^{-16}$	$2.45\cdot10^{-14}$

Table 3. Values of the cross-sections of the capture and recombination processes for electrons and hole, respectively. The work of the other investigators was for "ERL-type" configuration, while the present work is for the parallel plate configuration.

The increase in viscosity prevents the natural tendency of pure a-Se to crystallize over time, in terms of months to years, depending on the temperature and ambient conditions. However, doping with As has the negative effect of increasing the concentration of hole traps. A few parts per million (ppm) of

chlorine can be added to compensate for As-induced traps. The presence of the deep trapping states drastically affects the charge carriers' lifetimes, and thus determines the *Schubwegs.*

5.4 References

1. J. Kalade, E. Montrimas and J. Rakauskas, "The Mechanism of Sensitivity Reduction in Selenium Layers Irradiated by X-Rays", Phys. Stat. Sol. A **25** 629 (1974).

2. W. Que and J.A. Rowlands, "X-ray photogeneration in amorphous selenium: Geminate versus columnar recombination," Phys. Rev. B **51** 10500-10507 (1995).

3. D. M. Pai, R. C. Enck, "Onsager mechanism of photogeneration in amorphous selenium", Phys. Rev. B **11** (1975) 5163.

4. J. Hirsch and H. Jahankhani, "The carrier yield in a-Se under electron bombardment", J. Phys.: Condens. Matter **1** 8789 (1989).

5. M. Lachaine and B. G. Fallone, "Monte Carlo simulations of x-ray induced recombination in amorphous selenium", J. Phys. D: Appl. Phys. **33** 1417-23 (2000)

6. W. Zhao, G. DeCrescenzo, and J. A. Rowlands, "Investigation of lag and ghosting in amorphous selenium flat-panel X-ray detectors", Proc. SPIE **4682**, 9 (2002).

7. S. O. Kasap and V. Aiyah, "X-ray induced hole trapping in electroradiographic plates", J. Appl. Phys. **69**, 7087 (1991).

8. J. Rakauskas, J. Kalade and E. Montrimas, "The Fatigue Mechanism of X-Irradiated Amorphous Se Layer ", Liet. Fiz. Rink. **12** 611 (1972).

9. S. O. Kasap and C. Juhasz, "Time-of-flight drift mobility measurements on chlorine-doped amorphous selenium films", J. Phys. D **18** 703 (1985).

10. U. Schiebel, T. Buchkremer, G. Frings and P. Quadflieg, "Deep trapping and recombination in a-Se:As x-ray sensitive photoreceptors" J. Non-Cryst. Sol. **115**, 216 (1989).

11. S. O. Kasap, B. Fogal, M. Z. Kabir, R. E. Johanson, and S. O'Leary, "Recombination of drifting holes with trapped electrons in stabilized a-Se photoconductors: Langevin recombination", Appl. Phys. Lett. **84** 11 1991-1993 (2004).

12. S. O. Kasap and J. A. Rowlands, CDROM: "Optoelectronics and Photonics: Principles and Practices" (Prentice Hall, 2000).

Chapter 6: Conclusions

Experimentally, it has been verified that the mechanism of sensitivity reduction observed during the non-biased irradiation sequence can be accurately modeled by considering the trapping effect of photogenerated charge carriers, and recombination of trapped carriers with opposite free charge.

Comparing the biased and non-biased cases for different operating conditions, i.e. different air-kerma rates, electric fields and x-ray effective energies, we found that the sensitivity reduction effect is lower in the non-biased case. This shows that the electric field has a great influence on the mechanism of sensitivity reduction in a-Se detectors.

It has been observed that the sensitivity of a parallel plate a-Se detector for both the biased and non-biased cases drops substantially with an increase in air-kerma. This occurs because the concentration of the captured charge carriers on deep trapping sites increases with air-kerma. The reduction in sensitivity effect is greater for lower air-kerma rates and higher x-ray effective energies. It has also been shown that the sensitivity of a-Se increases with the increase of the applied electric field strength.

We also experimentally investigated the sensitivity recovery for both experimental sequences, i.e. biased and non-biased cases, corresponding to different fatiguing irradiation intervals. The mechanism of sensitivity recovery may consists in the release of charge carriers, i.e. electrons and holes, from deep trapping sites.

It was found that the sensitivity recovers faster for a detector irradiated to a large air-kerma than one which was irradiated to a smaller air-kerma, since the occupation of trapping sites increases with the level of air-kerma delivered. For the biased case, the recovery rate seems to be higher than for the non-biased case, but for the latter case there is less sensitivity to recover.

A theoretical model was developed to describe the mechanism of sensitivity reduction in the non-biased case of a parallel plate a-Se detector. We found good agreement between theory and experiment, for different operating conditions of the detector.

The density of traps responsible for the reduction in sensitivity process along with the trapping and recombination coefficients were determined by comparing theory to experiment for an externally biased a-Se layer. The values of these parameters are in good agreement with published data from associated "ERL-type" measurements in the literature. These parameters are intrinsic properties of a-Se and give us valuable inside information about the signal formation in the photodetector.

The dependence of sensitivity on the a-Se layer thickness for several x-ray effective energies was also calculated. The theoretical model predicts that the sensitivity peak shifts to higher values of the photodetector thickness with the increase in the effective photon energy. These trends are in good agreement with published data in literature for ERLs.

We believe that the experimental investigations and the theoretical calculations presented in this work are important in designing specifics within a-Se based detectors that can subsequently be used in megavoltage computed tomography (MVCT) and fluoroscopy where sensitivity-reduction may have significant effects.

Appendix

Detailed derivations of the equations involved in Section 4.1 are presented in Sections A.1 and A2. The derivation of the density of trapped charge carriers during the long irradiation intervals with the bias removed is presented in Section A.3.

A.1. Derivation of the normalized system of equations

A.1.1. Variation of the electric field across the photodetector thickness

Using the assumptions stated in Section 4.1 and the normalization given by Eq. (4.12), Eq. (4.1)

$$\frac{\partial E'(x',t')}{\partial x'} = \frac{e}{\varepsilon_0 \varepsilon}\left[m'_2(x',t') - m'_1(x',t') + p(x',t') - n(x',t')\right]$$

becomes

$$\frac{E_0}{l}\frac{\partial E(x,t)}{\partial x} = \frac{e}{\varepsilon_0 \varepsilon} M_0 \left[m_2(x,t) - m_1(x,t)\right]. \qquad \text{(a.1.1)}$$

Considering the definition of the constant a given by Eq. (4.19), we obtain Eq. (4.13)

$$\frac{\partial E(x,t)}{\partial x} = a\left[m_2(x,t) - m_1(x,t)\right].$$

A.1.2. Total current density

Equation (4.4)

$$J(t') = J_c(x',t') + \varepsilon_0 \varepsilon \frac{\partial E'(x',t')}{\partial t'}$$

becomes Eq. (4.18)

$$j(t) = j_c(x,t) + \frac{\partial E(x,t)}{\partial t}$$

after applying the normalization given by Eq. (4.12).

A.1.3. Rate equation for the density of trapped electrons

Using the assumptions stated in Section 4.1, replacing n and p from Eqs. (4.10) and (4.11), and by applying the normalization (4.12), Eq. (4.6)

$$\frac{\partial m'_1(x',t')}{\partial t'} = \gamma_{1n} n(x',t')\left[M_1 - m'_1(x',t')\right] - \gamma_{2h} p(x',t') m'_1(x',t')$$

transforms into

$$\frac{\partial m_1(x,t)}{\partial t} = t_0 \gamma_{1n}\left[1 - m_1(x,t)\right] - t_0 \gamma_{2h} m_1(x,t). \qquad \text{(a.1.2)}$$

From Eq. (4.12') we find that

$$t_0 = \frac{\varepsilon_0 \varepsilon E_0}{j_0}. \qquad \text{(a.1.3)}$$

Replacing Eq (a.1.3) into Eq. (a.1.2), and taking into account the coefficients given by Eq. (4.19), we obtain

$$\frac{\partial m_1(x,t)}{\partial t} = \frac{E_0}{j_0} e\mu_n \Gamma_{1n}\left[1 - m_1(x,t)\right] - \frac{E_0}{j_0} e\mu_p \Gamma_{2h} m_1(x,t) \qquad \text{(a.1.4)}$$

From Eq. (4.19) and the normalization given by Eq. (4.12) we obtain Eq. (4.15)

$$\frac{\partial m_1(x,t)}{\partial t} = \frac{j_n(x,t)}{E(x,t)} \Gamma_{1n}\left[1 - m_1(x,t)\right] - \frac{j_h(x,t)}{E(x,t)} \Gamma_{2h} m_1(x,t)$$

A.1.4. Rate equation for the density of trapped holes

Similarly as for the above derivation of Eq. (4.6), Eq. (4.5)

$$\frac{\partial m'_2(x',t')}{\partial t'} = \gamma_{1h} p(x',t')\left[M_2 - m'_2(x',t')\right] - \gamma_{2n} n(x',t') m'_2(x',t')$$

becomes

$$\frac{\partial m_2(x,t)}{\partial t} = t_0 \gamma_{1h}\left[1 - m_2(x,t)\right] - t_0 \gamma_{2n} m_2(x,t). \qquad \text{(a.1.5)}$$

Replacing Eq. (a.1.3) in Eq. (a.1.5) and taking into account the coefficients given by Eq. (4.19) we obtain

$$\frac{\partial m_2(x,t)}{\partial t} = \frac{E_0}{j_0} e\mu_n \Gamma_{1h}\left[1 - m_2(x,t)\right] - \frac{E_0}{j_0} e\mu_n \Gamma_{2n} m_2(x,t) \qquad \text{(a.1.6)}$$

Using Eq. (4.19) and the normalization given by Eq. (4.12) we obtain Eq. (4.14)

$$\frac{\partial m_2(x,t)}{\partial t} = \frac{j_h(x,t)}{E(x,t)} \Gamma_{1h}\left[1 - m_2(x,t)\right] - \frac{j_n(x,t)}{E(x,t)} \Gamma_{2n} m_2(x,t)$$

A.1.5. Variation of the current density of electrons across the photodector thickness

Normalizing Eq. (4.7)

$$\frac{\partial n(x',t')}{\partial t'} = \alpha_0 e^{-\mu x'} + \frac{1}{e}\frac{\partial J_{cn}(x',t')}{\partial x'} - \gamma_{1n} n(x',t')\left[M_1 - m'_1(x',t')\right] - \gamma_{2n} n(x',t') m'_2(x',t')$$

and using Eqs. (4.11) and (4.19) we obtain

$$\frac{\partial j_n(x,t)}{\partial x} = -\frac{el}{j_0}\alpha_0 e^{-\eta x} + \frac{el}{j_0}\frac{e\mu_n}{\varepsilon_0 \varepsilon} M_0 \left\{\Gamma_{1n}\left[1 - m_1(x,t)\right] + \Gamma_{2n} m_2(x,t)\right\}. \qquad \text{(a.1.7)}$$

Considering Eqs. (4.19) and (a.1.3) we find that

$$\frac{el\alpha_0}{j_0} = aQ. \qquad \text{(a.1.8)}$$

From Eqs. (4.10) and (4.19) we find

$$\frac{el}{j_0}\frac{e\mu_n}{\varepsilon_0 \varepsilon} M_0 = a\frac{j_n(x,t)}{E(x,t)}. \qquad \text{(a.1.9)}$$

Equating Eq. (a.1.7) with Eq. (a.1.9) we obtain Eq. (4.16)

$$\frac{\partial j_n(x,t)}{\partial x} = -aQe^{-\eta x} + a\frac{j_n(x,t)}{E(x,t)}\left\{\Gamma_{1n}\left[1-m_1(x,t)\right]+\Gamma_{2n}m_2(x,t)\right\}. \qquad \text{(a.1.10)}$$

A.1.6. Variation of the current density of holes across the photodetector thickness

For Eq. (4.8)

$$\frac{\partial p(x',t')}{\partial t'} = \alpha_0 e^{-\mu x'} - \frac{1}{e}\frac{\partial J_{ch}(x',t')}{\partial x'} - \gamma_{1h}p(x',t')\left[M_2 - m'_2(x',t')\right] - \gamma_{2h}p(x',t')m'_1(x',t')$$

we apply a similar method as for Eq. (4.7) and find

$$\frac{\partial j_n(x,t)}{\partial x} = -\frac{el}{j_0}\alpha_0 e^{-\eta x} + \frac{el}{j_0}\frac{e\mu_p}{\varepsilon_0\varepsilon}M_0\left\{\Gamma_{1h}\left[1-m_2(x,t)\right]+\Gamma_{2h}m_1(x,t)\right\}. \qquad \text{(a.1.11)}$$

From Eqs. (4.11) and (4.19) we obtain

$$\frac{el}{j_0}\frac{e\mu_h}{\varepsilon_0\varepsilon}M_0 = a\frac{j_h(x,t)}{E(x,t)}. \qquad \text{(a.1.12)}$$

Considering Eqs. (a.1.8) and (a.1.12), Eq. (a.1.11) becomes Eq. (4.17)

$$\frac{\partial j_h(x,t)}{\partial x} = aQe^{-\eta x} - a\frac{j_h(x,t)}{E(x,t)}\left\{\Gamma_{2h}m_1(x,t)+\Gamma_{1h}\left[1-m_2(x,t)\right]\right\}. \qquad \text{(a.1.13)}$$

A.2 Derivation of the initial current densities

A.2.1. Current density of electrons

We start with Eq. (4.16)

$$\frac{\partial j_n(x,t)}{\partial x} = -aQe^{-\eta x} + a\frac{j_n(x,t)}{E(x,t)}\left\{\Gamma_{1n}\left[1-m_1(x,t)\right]+\Gamma_{2h}m_2(x,t)\right\}.$$

We replace the solution given by Eq. (4.20) for j_n into Eq. (4.16), then using Eq. (4.21) we obtain

$$\frac{dj_{n0}(x)}{dx} + t\frac{dj_{n1}(x)}{dx} = -aQe^{-\eta x} + a\frac{\left[j_{n0}(x)+t\cdot j_{n1}(x)\right]}{(1+tE_1)} \times\left\{\left[\Gamma_{2h}m+\Gamma_{1n}(1-m)\right]+t\left[\Gamma_{2h}m_{11}(x)-\Gamma_{1h}m_{11}(x)\right]\right\} \quad \text{(a.2.1)}$$

In order to determine j_{n0}, we replace $t=0$ in the above equation and obtain

$$\frac{\partial j_{n0}(x)}{\partial x} = -aQe^{-\eta x} + aj_{n0}(x)[\Gamma_{1n}(1-m)+\Gamma_{2h}m] \quad \text{(a.2.2)}$$

Considering Eq. (4.29), Eq. (a.2.2) becomes

$$\frac{dj_{n0}(x)}{dx} = -aQe^{-\eta x} + g_n j_{n0}(x). \quad \text{(a.2.3)}$$

We now solve the first order differential equation

$$\frac{d}{dx}\left[j_{n0}(x)e^{-g_n x}\right] = -aQe^{-(g_n+\eta)x} \quad \text{(a.2.4)}$$

and obtain

$$j_{n0}(x) = j_{n0}(0)e^{g_n x} + \frac{aQ}{(\eta + g_n)}\left[e^{-\eta x} - e^{g_n x}\right] \tag{a.2.5}$$

Considering Eq. (4.22), Eq. (a.2.5) becomes

$$j_{n0}(0) = \frac{aQ}{(\eta + g_n)}\left[1 - e^{-(\eta + g_n)}\right]. \tag{a.2.6}$$

Replacing Eq. (a.2.6) into (a.2.5) we obtain Eq. (4.28)

$$j_{n0}(x) = \frac{aQ}{(\eta + g_n)}\left[e^{-\eta x} - e^{-(\eta + g_n)}e^{g_n x}\right].$$

A.2.2. Current density of holes

Similarly as for the current density of electrons, we start with Eq. (4.17)

$$\frac{\partial j_h(x,t)}{\partial t} = aQe^{-\eta x} - a\frac{j_h(x,t)}{E(x,t)}\left\{\Gamma_{2h}m_1(x,t) + \Gamma_{1h}\left[1 - m_2(x,t)\right]\right\}$$

and after following the steps described above we obtain

$$\frac{dj_{p0}(x)}{dx} = aQe^{-\eta x} - g_p j_{p0}(x). \tag{a.2.7}$$

We now solve the first order differential equation

$$\frac{d}{dx}\left[j_{p0}(x)e^{-g_p x}\right] = aQe^{(g_p - \eta)x} \tag{a.2.8}$$

Considering Eq. (4.22), the solution of Eq. (a.28) gives us Eq. (4.27)

$$j_{h0}(x) = \frac{aQ}{(g_h - \eta)}\left(e^{-\eta x} - e^{-g_h x}\right).$$

A.3. Kinematics in the photodetector layer with no electric field applied

The kinetics of sensitivity reduction effect, in the absence of an external electric field, is described by the following system of equations[1]

$$\frac{\partial n(x,t)}{\partial t} = \alpha_0 \, e^{-\mu x} - \gamma'_{1n}\left[M_1 - m_1(x,t)\right]n(x,t) - \gamma'_{2n}\, m_2(x,t)n(x,t) \qquad \text{(a.3.1)}$$

$$\frac{\partial m_1(x,t)}{\partial t} = \gamma'_{1n}\, n(x,t)\left[M_1 - m_1(x,t)\right] - \gamma'_{2n}\, p(x,t)m_1(x,t) \qquad \text{(a.3.2)}$$

$$\frac{\partial p(x,t)}{\partial t} = \alpha_0 \, e^{-\mu x} - \gamma'_{1h}\left[M_2 - m_2(x,t)\right]p(x,t) - \gamma'_{2h}\, m_1(x,t)p(x,t) \qquad \text{(a.3.3)}$$

$$\frac{\partial m_2(x,t)}{\partial t} = \gamma'_{1h}\, p(x,t)\left[M_2 - m_2(x,t)\right] - \gamma'_{2h}\, n(x,t)m_2(x,t) \,. \qquad \text{(a.3.4)}$$

These equations describe the kinetics of the charge carriers in a-Se during the long (fatiguing) irradiation intervals. By solving the above system of partial differential equations we determine the density of trapped charge during subsequent fatiguing irradiation intervals. Then this relation is used to determine the reduction in sensitivity with the increase in air-kerma delivered to the a-Se layer.

The definitions of symbols in Eqs. (a.3.1) – (a.3.4) are the same as in Eqs. (3) – (6) except that the variables γ'_{1n}, γ'_{1h}, γ'_{2n}, and γ'_{2h} are the trapping and

recombination coefficients for electrons and holes in the absence of the electric field. Generally, these coefficients may change in the presence of an electric field, hence γ'_{1n}, γ'_{1h}, γ'_{2n}, and from Eqs. (a.3.1) – (a.3.4) replace the parameters γ_{1n}, γ_{1h}, γ_{2n}, and γ_{2h} from Eqs. (3) – (6) that had been designed for the case of an external bias.

In order to simplify the Eqs. (a.3.1) – (a.3.4) one can assume that the photo-detector layer is neutral[2] before irradiation, therefore $n+m_1=p+m_2$. Experimentally, it has been shown that this relationship is valid during the irradiation process[3]. Hence, it can be assumed that the trapping densities of the charge carriers are equal and constant, i.e. $m_1=m_2=m$, and $n=p$. Therefore, by substituting $n=p$, equating (a.3.1) with (a.3.3) and comparing terms containing m, we can obtain the following identities

$$\gamma'_{1n}+\gamma'_{2n}=\gamma'_{1h}+\gamma'_{2h},\ \gamma'_{1n}M_1=\gamma'_{1h}M_2. \tag{a.3.5}$$

Further simplification can be obtained in solving this system of equations by assuming that $M_1=M_2=M_0=\text{const}$.

From Eq. (a.3.5), we then obtain the following equalities $\gamma'_{1n}=\gamma'_{1h}$, $\gamma'_{2n}=\gamma'_{2h}$. Eqs. (a1) and (a2) become

$$\frac{\partial n(x,t)}{\partial t}=\alpha(x)-\gamma'_{1n}\left[M_0-m(x,t)\right]n(x,t)-\gamma'_{2n}m(x,t)n(x,t) \tag{a.3.6}$$

$$\frac{\partial m(x,t)}{\partial t}=\gamma'_{1n}n(x,t)\left[M_0-m(x,t)\right]-\gamma'_{2n}n(x,t)m(x,t) \tag{a.3.7}$$

where $\alpha(x)=\alpha_0 e^{-\mu x}$.

The solution of m obtained from Eq. (a.3.7) is given by

$$m(x,t)=\frac{\gamma'_{1n}M_0}{\gamma'_{1n}+\gamma'_{2n}}\left\{1-\exp\left[-(\gamma'_{1n}+\gamma'_{2n})\int_0^t n(x,t')dt'\right]\right\} \tag{a.3.8}$$

The maximum value of m is given by

$$m_{\max}=\frac{\gamma'_{1n}M_0}{\gamma'_{1n}+\gamma'_{2n}}.$$

In the above equation $m_{\max}\neq M_0$ for $\gamma'_{2n}\neq 0$, therefore the trapping levels can not be fully occupied because of the recombination process. The analytical solution of Eqs. (a.3.6) and (a.3.7) can be found for the case when $\gamma'_{1n}=\gamma'_{2n}=\gamma$. With this simplification, Eq. (a.3.6) becomes

$$\frac{\partial n(x,t)}{\partial t}+\gamma M_0 n(x,t)=\alpha(x). \tag{a.3.9}$$

The solution of Eq. (a.3.9) is given as follows

$$n(x,t)=\frac{\alpha(x)}{\gamma M_0}\left(1-e^{-\gamma M_0 t}\right),\ t\le T_0 \tag{a.3.10}$$

where T_0 is the total time of each long irradiation.

Substituting Eq. (a.3.10) in (a.3.8), and integrating for x we obtain the following solution for the trapped charge

$$m(t)=\frac{M_0}{2}\left\{1-\exp\left[-\frac{2\alpha_1}{M_0}\left(t-\frac{1-e^{-\gamma M_0 t}}{\gamma M_0}\right)\right]\right\},\ t\le T_0 \tag{a.3.11}$$

where (see Appendix A.4)

$$\alpha_1 = \frac{5.45 \cdot 10^{13}}{W_{\pm}} \frac{\gamma_{Se}}{\gamma_0} \dot{K} \frac{1 - e^{-\eta}}{\eta}.$$

Furthermore, from Eq. (a.3.9) and condition $\alpha(x) = 0$ for $t \geq T_0$ we obtain the following solution for $n(x,t)$ as given by

$$n(x,t) = \frac{\alpha(x)}{\gamma M_0}\left(e^{\gamma M_0 T_0} - 1\right)e^{-\gamma M_0 t} \qquad \text{(a.3.12)}$$

Substituting Eq. (a.3.12) in (a.3.8) and integrating for x, the solution for the trapped charge is given as follows

$$m(t) = \frac{M_0}{2}\left\{1 - \exp\left[\frac{2\alpha_1}{M_0}\left(\frac{e^{\gamma M_0 T_0} - 1}{\gamma M_0} e^{-\gamma M_0 t} - T_0\right)\right]\right\} \qquad \text{(a.3.13)}$$

The relationship between the total air-kerma K, and the number of electron-hole pairs generated by the x-ray interactions per unit volume and time is written as follows[1]

$$\varphi K = \frac{2\alpha_1 T_0}{M_0}. \qquad \text{(a.3.14)}$$

In Eq. (a.3.14) φ is a proportionality factor that does not depend on air-kerma, and is determined by the quantum efficiency, radiation hardness and the concentration of deep trapping sites.

For the case $\gamma M_0 T_0 >> 1$ and by performing Taylor expansions Eq. (a.3.13) simplifies to the following

$$m = \frac{M_0}{2}\left(1 - e^{-\varphi K}\right), \; t \geq T_0. \qquad \text{(a.3.15)}$$

This relation shows the relationship of trapped charge carriers and air-kerma, and is used in deriving the sensitivity for the case of electric field. Rakauskas *et al*[1] showed that Eq. (a.3.15) is also a good approximation of the case $\gamma'_{1n} \neq \gamma'_{2n}$.

A.4 Photogeneration rate

The x-ray photons are absorbed exponentially as $\exp(-\mu x)$ along the layer thickness and generate EHPs. If E_{eff} is the x-ray effective energy and $\dot{N}_0$ is the rate of x-ray photons per unit area incident on the photodetector, then the initial hole or electron concentration rate at location x in the a-Se layer is given by[4]

$$\alpha_0 = \frac{E_{eff}\dot{N}_0\gamma_{Se}}{W_{\pm}}\exp(-\mu x) \qquad \text{(a.4.1)}$$

where γ_{Se} is the mass energy absorption coefficient of a-Se and $W_{\pm}$ is the average energy required to create a collectable EHP.

The incident x-ray photons per unit area, i.e. N_0, is given by[5]

$$N_0 = \frac{5.45\times10^{13}K}{E_{eff}\gamma_{air}} \qquad \text{(a.4.2)}$$

where γ_{air} is the mass energy absorption coefficient of air, and K is the air-kerma.

Replacing Eq. (a.4.2) into Eq. (a.4.1) we obtain

$$\alpha_0 = \frac{5.45\cdot10^{13}}{W_{\pm}}\frac{\gamma_{Se}}{\gamma_0}\dot{K}\ (cm^{-3}s^{-1}) \qquad \text{(a.4.3)}$$

where $\dot{K}$ is the air-kerma rate.

A.5 References

1. J. Rakauskas, J. Kalade and E. Montrimas, "The Fatigue Mechanism of X-Irradiated Amorphous Se Layer ", Liet. Fiz. Rink. **12** 611 (1972).

2. S. O. Kasap and J. A. Rowlands, CDROM: "Optoelectronics and Photonics: Principles and Practices" (Prentice Hall, 2000).

3. J. Kalade, E. Montrimas and J. Rakauskas, "Se Electroradiographic Layers Discharge Mechanism in Case of X-ray Irradiation", Liet. Fiz. Rink. **12** 597 (1972).

4. M. Z. Kabir and S.O. Kasap, "Charge collection and absorption-limited sensitivity ox x-ray photoconductors: Application to a-Se and HgI_2", Appl. Phys. Lett. **80** 1664 (2002).

5. J. M. Boone, "Handbook of Medical Imaging", edited by J. Beutel, K. L. Kundel, and R. L. Van Metter, (SPIE Press, Washington, 2000), Vol. 1, Chap. 1.

Bibliography

1. M. A. Abkowitz in Disordered Semiconductors, M. A. Kastner, G. A. Thomas, S. R. Ovshinsky, eds., Plenum Publishing, New York (1987), p. 205. [p. 15, 30]

2. M. Abkowitz, "Density of states in a-Se from combined analysis of xerographic potentials and transient transport data," Philos. Mag. Lett. **58** (1), 53-57 (1988). [p. 30, 57]

3. Abkowitz M. A., "Disordered Semiconductors", ed. Kastner M. A., Thomas G. A., and Ovshinsky S. R. (Plenum Publishing Co., New York, 1978) p. 205, and references therein. [p. 24, 31]

4. M. Abkowitz and J. M. Markovics, "Evidence of equilibrium native defect populations in amorphous chalcogenides from analyses of xerographic spectra", J. Non-Cryst. Solids **66** 315 (1984). [p. 24, 31]

5. M. Abkowitz and R. C. Enck, "Xerographic Spectroscopy of Localized Electronic States in Amorphous Semiconductors", Phys. Rev. B **25** 2567 (1982). [p. 56]

6. Adler D., "Amorphous Semiconductor Devices", Sci. Am. **36** 236 (1977). [p. 31]

7. L.E. Antonuk, Y. El-Mohri, J.H. Siewerdsen and J. Yorkston, "Empirical investigation of the signal performance of a high-resolution, indirect detection,

active matrix flat-panel imager (AMFPI) for fluoroscopic and radiographic operation," Med. Phys. **24** 51-70 (1997). [p. 14, 28]

8. L.E. Antonuk, Y. El-Mohri, W. Huang, K.-W. Jee, J. Siewerdsen, M. Maolinbay, V. Scarpine, H. Sandler and J. Yorkston, "Initial Performance Evaluation of an indirectdetection, active matrix flat-panel imager (AMFPI) prototype for megavoltage imaging," Int. J. Rad. Onc. Biol. Phys. **42** 437-452 (1998). [p. 15, 28]

9. I.P. Batra, K.K. Kanazawa and H. Seki, "Discharge Characteristics of Photoconducting Insulators", J. Appl. Phys. **43** 4, 1845-53 (1972). [p. 56]

10. I.M. Blevis, D.C. Hunt and J.A. Rowlands, "Measurement of x-ray photogeneration in amorphous selenium," J. Appl. Phys. **85** 7958-7963 (1999). [p. 29]

11. A. Brauers, N. Conrads, G. Frings, U. Schiebel, M. J. Powell, and C. Glasse, "Charge Collection in a Se Photoconductor on a Thin Film Transistor Array During X-ray Imaging", Mat. Res. Soc.Symp. Proc. **467** 919-924 (1997). [p. 56]

12. S. Chand, R. C. Bhatheja, G. D. Sharma, and S. Chandra, "Deep intrinsic and photostructural defects levels in amorphous selenium films", J. Appl. Phys. **70** (9) (1991) 5122-5124. [p. 31]

13. 54. S. Chand, R. C. Bhatheja, G. D. Sharma, and S. Chandra, "Effect of chlorine doping on photostructural defect states in amorphous selenium films", Appl. Phys. Lett. **59** (27) (1991) 3514-3515. [p. 31]

14. H. G. Chotas et al, "Memory Artifacts Related to Selenium-based Digital Radiograph Systems", Radiology VOL. **203** No. 3 pp. 881-883 1997. [p. 15, 30]

15. S. R. Elliott, "Physics of Amorphous Solids" (Longman, London, UK, 1992). [p. 31]

16. E. Fourkal, M. Lachaine, and B. G. Fallone, "Signal formation in amorphous-Se-based x-ray detectors", Phys. Rev. B **63** 195204. [p. 13, 29]
17. C. Haugen and S. O. Kasap, "X-ray irradiation induced bulk space charge in stbilized a-Se x-ray photoconductors", J Appl. Phys. **84** 5495, (1998). [p. 55]

18. C. J. Haugen, X-ray Photoconductivity (1999). [p. 28]

19. J. Hirsch and H. Jahankhani, "The carrier yield in a-Se under electron bombardment", J. Phys.: Condens. Matter **1** 8789 (1989). [p. 29, 76]

20. G. Jaffé, "Columnar ionization," Le Radium **10** 126-134 (1913). [p. 29]

21. Kalade J. et al, "The deep localised state energetical distribution in a-Se and a-Si:H layers", Proc. SPIE **2780** (1996) 206-209. [p. 31]

22. J. Kalade, E. Montrimas and J. Rakauskas, "Se Electroradiographic Layers Discharge Mechanism in Case of X-ray Irradiation", Liet. Fiz. Rink. **12** 597 (1972). [p. 55, 92]

23. J. Kalade, E. Montrimas and J. Rakauskas, "The Mechanism of Sensitivity Reduction in Selenium Layers Irradiated by X-Rays", Phys. Stat. Sol. A **25** 629 (1974). [p. 31, 55, 76]

24. A. I. Kaminskas and I. Sidaravichus, "Physical and Technoogical Aspects of Electroradiography", Sci. Appl. Photo. **35** 624 (1994). [p. 55]

25. K.K. Kanazawa and I.P. Batra, "Deep-Trapping Kinematics", J. Appl. Phys. **43** 4, 1845-53 (1972). [p. 56]

26. S. O. Kasap and J. A. Rowlands, CDROM: "Optoelectronics and Photonics: Principles and Practices" (Prentice Hall, 2000). [p. 42, 77, 92]
27. Kasap S. O., "The Handbook of Imaging Materials", ed. A. Diamond (Marcel Dekker, New York, 1991) ch. 8 and references therein. [p. 15, 30]

28. S. O. Kasap, V. Aiyah, B. Polischiuk, A. Bhattacharyya, and Z. Liang, "Deep-trapping kinematics of charge carriers in amorphous semiconductors: A theoretical and experimental study", Phys. Rev. B **43** 8, 6691-6705 (1991). [p. 56]

29. S. O. Kasap and V. Aiyah, "X-xay induced hole trapping in electroradiographic plates", J. Appl. Phys. **69**, 7087 (1991). [p. 55, 76]

30. S. O. Kasap, B. Fogal, M. Z. Kabir, R. E. Johanson, and S. O'Leary, "Recombination of drifting holes with trapped electrons in stabilized a-Se photoconductors: Langevin recombination", Appl. Phys. Lett. **84** 11 1991-1993 (2004). [p. 56]

31. S. O. Kasap, B. Fogal, M. Z. Kabir, E. Johanson, and S. O'Leary, "Recombination of drifting holes with trapped electrons in stabilized a-Se photoconductors: Langevin Recombination", Appl. Phys. Lett. **84** 11 1991-1993 (2004). [p. 77]

32. S. O. Kasap and V. Aiyah, "X-Ray induced hole trapping in electroradiographic plates", J. Appl. Phys. **69**, 7087 (1991). [p.]

33. S. O. Kasap and C. Juhasz, "Time-of-flight drift mobility measurements on chlorine-doped amorphous selenium films", J. Phys. D **18** 703 (1985). [p. 76]

34. M. Kastner and D. Adler, "Valence-Alternation Model for Localized Gap States in Lone-Pair Semiconductors", Phys. Rev. Lett. **37**, 1504 (1976). [p. 56]

35. C.A. Klein, "Band gap dependence and related features of radiation ionization energies in semiconductors," J. Appl. Phys. **39** 2029 (1968). [p. 27]

36. H.A. Kramers, "On a modification of Jaffé's theory of column ionization," Physica (Utrecht) **18** 665-675 (1952). [p. 29]

37. M. Lachaine and B. G. Fallone, "Monte Carlo simulations of x-ray induced recombination in amorphous selenium", J. Phys. D: Appl. Phys. **33** 1417-23 (2000). [p. 76]

38. M. Lachaine, "Portal Imaging with a Direct-Detection Active Matrix Flat Panel Imager", PhD Thesis (2001). [p. 13, 29]

39. M. Lachaîne, E. Fourkal, and B. G. Fallone, "Investigation into the physical characteristics of active matrix flat panel imagers for radiotherapy," Med. Phys. **28** (8), 1689-1695 (2001). [p. 14, 27]

40. M. Lachaîne, E. Fourkal, and B. G. Fallone, "Detective quantum efficiency of a direct-detection active matrix flat panel imager at megavoltage energies," Med. Phys. **28** (7), 1364-1372 (2001). [p. 14, 27]

41. P. Langevin, "Recombinaison et mobilités des ions dans les gaz," Ann. Chim. Phys.
28 287-433 (1903). [p. 46, 50, 56]

42. D. Mah, J.A. Rowlands and J.A. Rawlinson, "Sensitivity of amorphous selenium to x-rays from 40 kVp to 18 MV: Measurements and implications for portal imaging,"
Med. Phys. **25** 444-456 (1998). [p. 15, 27]

43. Own A. E. and Marshall J. M., Proceedings on the Seventh International Conference on Amorphous and Liquid Semiconductors, Edinburgh (1977) p. 529. [p. 30]

44. D. M. Pai, R. C. Enck, "Onsager mechanism of photogeneration in amorphous selenium", Phys. Rev. B **11** (1975) 5163. [p. 29, 76]

45. G. Pang, D. L. Lee, and J. A. Rowlands, "Investigation of a direct conversion flat panel imager for portal imaging," Med. Phys. **28** (10), 2121-2128 (2001). [p. 13, 27]

46. B. Polischuk, H. Rougeot, K. Wong, A. Debrie, E. Poliquin, M. Hansroul, J. Martin, T. Truong, M. Choquette, L. Laperrière, and Z. Shukri, "Direct conversion detector for digital mammography," Proc. SPIE **3659**, 417-425 (1999). [p. 14, 27]

47. W. Que and J.A. Rowlands, "X-ray photogeneration in amorphous selenium: Geminate versus columnar recombination," Phys. Rev. B **51** 10500-10507 (1995). [p. 28, 76]

48. J. Rakauskas, J. Kalade and E. Montrimas, "The Fatigue Mechanism of X-Irradiated Amorphous Se Layer ", Liet. Fiz. Rink. **12** 611 (1972). [p. 55, 76, 92]

49. J. A. Rowlands, S. O. Kasap, "Amorphous Semiconductors Usher in Digital X-ray Imaging", Phys. Today 50 (11), 24-30 (1997). [p. 42]

50. E. Samei and M. J. Flynn, "An experimental comparison of detector performance for direct and indirect digital radiography systems," Med. Phys. **30** (4), 608-622 (2003). [p. 13, 27]

51. R. M. Schaffert, R. C. McMaster, and W. E. Bixby, "Electroradiography," U.S. Patent 2666144 (1950). [p. 13, 28]

52. U. Schiebel, T. Buchkremer, G. Frings and P. Quadflieg, "Deep trapping and recombination in a-Se:As x-Ray sensitive photoreceptors" J. Non-Cryst. Sol. **115**, 216 (1989). [p. 55, 77]

53. C. Schroeder, T. Stanescu, S. Rathee and B. G. Fallone, "Lag paper", Med. Phys (2004). [p. 15, 30]

54. J.H. Siewerdsen, L.E. Antonuk, Y. El-Mohri, J. Yorkston, W. Huang and J.M. Boudry, "Empirical and theoretical investigation of the noise performance of indirect detection, active matrix flat-panel imagers (AMFPIs) for diagnostic radiology," Med. Phys. **24** 71-89 (1997). [p. 14, 28]

55. J.H. Siewerdsen, L.E. Antonuk, Y. El-Mohri, J. Yorkston and W. Huang, "Signal, noise power spectrum, and detective quantum efficiency of indirect-detection flat-panel imagers for diagnostic radiology," Med. Phys. **25** 614-628 (1998). [p. 14, 28]

56. H.-Z. Song, G. J. Adriaenssens, E. V. Emelianova, and V. I. Arkhipov, "Distribution of gap states in amorphous delenium thin films", Phys. Rev. B **59** (1999) 10610. [p. 23, 30, 57]

57. S. Steciw, T. Stanescu, S. Rathee, and B. G. Fallone, "Sensitivity Reduction in Biased Amorphous Selenium Photoconductors", J. Phys. D: Appl. Phys. **35**, 1 (2002). [p. 15, 30, 42, 55]

58. P. Stavrev, A. Niemierko, N. Stavreva, and M. Goitein, "The Application of Biological Models to Clinical Data", Physica Medica **17** (2001). [p. 57]

59. S. M. Sze, "Physics of Semiconductor Devices", 2nd edition, John Wiley & Sons Inc., 1981, pg. 51. [p. 56]

60. A. Tsukamoto, S. Yamada, T. Tomisaki, M. Tanaka, T. Sakaguchi, H. Asahina, and M. Nishiki, "Development of a selenium-based flat-panel detector for real-time radiography and fluoroscopy," Proc. SPIE **3336**, 388-395 (1998). [p. 14, 29]

61. Wong C. K. et al, J. Non-Cryst. Solids **1171** 97-98 (1985). [p. 31]

62. Veres J. and Juhasz C., J. Non-Cryst. Solids **407** 164-166 (1993). [p. 31]

63. W. Zhao, W. G. Ji, A. Debrie, and J. A. Rowlands, "Imaging performance of amorphous selenium based flat-panel detectors for digital mammography: Characterization of a small area prototype detector," Med. Phys. **30** (2), 254-263 (2003). [p. 13, 27]

64. W. Zhao, I. Blevis, S. Germann and J.A. Rowlands, "Digital radiology using active matrix readout of amorphous selenium: Construction and evaluation of a prototype realtime detector," Med. Phys. **24** 1834-1843 (1997). [p. 13]

65. Zhao and J.A. Rowlands, "X-ray imaging using amorphous selenium: Feasibility of a flat panel self-scanned detector for digital radiology," Med. Phys. **22** 1595-1604 (1995). [p. 13, 29]

66. W. Zhao and J.A. Rowlands, "Digital radiology using active matrix readout of amorphous selenium: Theoretical analysis of detective quantum efficiency," Med. Phys. **24** 1819-1833 (1997). [p. 28, 29]

67. W. Zhao, G. DeCrescenzo, and J. A. Rowlands, "Investigation of lag and ghosting in amorphous selenium flat-panel X-ray detectors", Proc. SPIE **4682**, 9 (2002). [p. 15, 30, 55, 76]